NTNU

Norwegian University of
Science and Technology

The State of Minimum Entropy Production in Hydrogen Liquefaction

Ragnhild Aaraas Hånde

Master of Science in Physics and Mathematics
Submission date: June 2018
Supervisor: Jon Andreas Støvneng, IFY
Co-supervisor: Øivind Wilhelmsen, SINTEF Energi

Norwegian University of Science and Technology
Department of Physics

Preface

This thesis was submitted to the Department of Physics, Faculty of Natural Sciences, Norwegian University of Science and Technology (NTNU). This thesis is a part of my masters degree in applied physics, which is a five-year education program at the NTNU.

The work on this thesis was limited to 20 weeks, from the beginning of January to the beginning of June 2018. My supervisor was Adjunct Professor Øivind Wilhelmsen (Department of Energy and Precess Technology and SINTEF Energy Research).

Abstract

The main object of this thesis is to understand how to improve the hydrogen liquefaction process, by studying energy efficient heat exchanger design. This study is limited to the low temperature cooling (cryogenic cooling) of hydrogen gas from about 47K to 29K. The energy efficient heat exchanger design is found by minimizing the entropy production. A plate fin heat exchanger with catalyst pellets in some of the layers is used. In this heat exchanger there are three sources of entropy production: The heat transfer through the walls of the heat exchanger, the spin-isomer conversion reaction and the pressure drop.

This thesis presents optimal cooling strategies for two hydrogen heat exchangers operating at different conditions. The optimal cooling strategy is defined as the temperature profile of the cooling medium resulting in a minimum produced entropy. The first heat exchanger is operating at about 20 bar and the second is operating at about 80 bar.

The optimal paths are compared to reference cases. In the reference cases, hydrogen gas is used as cooling medium (refrigerant). The optimal cooling strategies are obtained by using optimal control theory. In the optimization, there are no restrictions on what temperatures the cooling medium may take. All boundary conditions are fixed, except the outlet pressure.

The optimization resulted in an improvement in total entropy production of 14.90% in the 20 bar case. In the 80 bar case, the improvement is 2.15%. This finding indicates that hydrogen, the baseline reference, could be an good choice of refrigerant in this particular 80 bar case.

The optimizations also show that the heat transfer and the hydrogen spin-isomer reaction are the most important sources of entropy production, and that they are almost equally important throughout the entire heat exchanger in both cases. This is due to the slow nature of the hydrogen spin-isomer reaction, which makes the hydrogen heat exchanger different from other reactors/heat exchangers studied in literature. In literature, optimal reactors/heat exchangers have been characterized by a reaction mode and a heat transfer mode. These modes are not present in our hydrogen liquefier. However, we have found that Eivind Johannessens hypothesis concerning equipartition of entropy production and forces in systems with too few control variables, to some degree applies to this system. In the 20 bar case there is only a 2.39% deviation between the total entropy production in the equipartition of entropy production state and the optimal state.

Sammendrag

Målet med denne oppgaven er å forstå hvordan man kan forbedre prosessen for flytendegjøring av hydrogen ved å studere energieffektivt varmeveksler design. Denne oppgaven er begrenset til lavtemperatur nedkjøling av hydrogengass fra rundt 47K til 29K. Energieffektiv varmevekslerdesign finnes ved å minimere entropiproduksjonen. Varmeveksleren i studien er av type plate-finne. Det er tre kilder til entropiproduksjons i varmeveksleren: Varmeoverføring gjennom varmeveksler veggene, hydrogen spinn-isomer reaksjonen og trykkfallet gjennom varmeveksleren.

Denne oppgaven presenterer to optimale nedkjølingsstrategier for hydrogen i plate-finne-varmeveksler. De to varmevekslerene i studien opererer ved trykk på henholdsvis 20 og 80 bar. Optimale nedkjølingsstrategier er i denne sammenhengen definert som temperaturprofilen til kjølemediet på utsiden av varmeveksleren som gir lavest entropiproduksjon.

Optimale nedkjølingsstrategier blir sammenliknet med en referansetilstand. I referansetilstanden brukes hydrogengass som kjølemedium. De optimale nedkjølingsstrategiene ble funnet ved å bruke optimal kontrollteori. Det er ingen begrensinger på hvilke temperaturer kjølemediet kan ta i optimeringen. Alle grensebetingelser er fiksert, bortsett fra trykket ved utløpet av varmeveksleren.

Optimeringen førte til en reduksjon i total entropiproduksjon på 14.90% i 20 bar-tilfellet og 2.15% i 80 bar-tilfellet. Funnet indikerer at hydrogen vil i 80 bar-tilfellet være et godt nedkjølingsmedium.

Videre viser optimeringen at de to viktigste kildene til entropiproduksjon i varmevekslerene er varmeoverføring gjennom veggene og spinn-isomer reaksjonen og at de to entropiproduksjonsbidragene er omtrent like store gjennom hele varmeveksleren i begge tilfellene. Årsaken til dette er at hydrogen spinn-isomer reaksjonen er en relativt treg reaksjon. Dette fører til at varmeveksleren får andre egenskaper enn reaktorer studert tidligere, hvor man har sett at den optimale løsningen kan karakteriseres ved et reaksjonsmodus og et varmeoverføringsmodus. Disse to modusene er ikke observert i vår varmeveksler. Det vi derimot har observert er at Eivind Johannessens hypotese om ekvipartisjon av entropiproduksjon og ekvipartisjon av krefter i systemer med for få kontrollvariabler, vil til en viss grad gjelde for hydrogenvarmeveksleren. Spesielt i 20 bar-tilfellet, hvor ekvipartisjon av entropiproduksjon resulterer i en total entropiproduksjon som kun avviker med 2.39% fra den optimale.

Acknowledgement

I want to thank my supervisor Øivind Wilhelmsen. As my only supervisor in this study, Øivind has guided and motivated me through my thesis work. Thank you for being patient with me. I want to thank Eivind Johannessen for making a thorough and structured entropy minimization Matlab code and helping me analyzing my results.

I also want to thank David Berstad for providing me with reference data on the heat exchanger, and I want to thank the HYPER project for financing a trip to London to meet Øivind.

I will also thank Andreas Dørum (my boyfriend), for making me dinner and for being a good listener and I want to thank my colleges at fysikkland for great lunch breaks and inspirational talks. Finlay, I want to thank my parents for always supporting me and for being good role models and infinite sources of inspiration.

Contents

List of Figures

List of Tables

Chapter 1

Introduction

In December 2015, 195 nations committed to the Paris agreement. This was the first universal binding climate-deal. The agreement commits the nations to a plan of action: The global warming must not exceed maximum of 2 degrees [1]. Fossil fuels are great contributors to global warming. This is why it is important to find attractive alternatives, which in the future can replace all fossil fuels.

1.1 Motivation

According to the US Energy Information Administration, the worlds energy consumption will increase by 28% from 2015 to 2040 [2].

Today, fossil fuels, such as gas, oil and coal are our main energy sources. According to BP Statistical Review of World Energy from 2017, fossil fuels stand for more than 80% of our consumption, where renewables stand for only 3.2% [3]. The International Energy Agency

(IEA) states in the Energy Technology Perspective 2015 that

> The energy intensity of global gross domestic product (GDP) and the carbon intensity of primary energy both have to be reduced by around 60% by 2050 in the 2°C Scenario (2DS) on a global level compared with today [4].

The Energy Technology Perspective 2015 [4] mentions hydrogen as an important component for reducing the CO_2 emissions. Hydrogen is an energy carrier, which can be used as a zero-emission fuel. The only bi-products of the hydrogen fuel cell are water and heat. This makes hydrogen an attractive replacement for gasoline used in transportation.

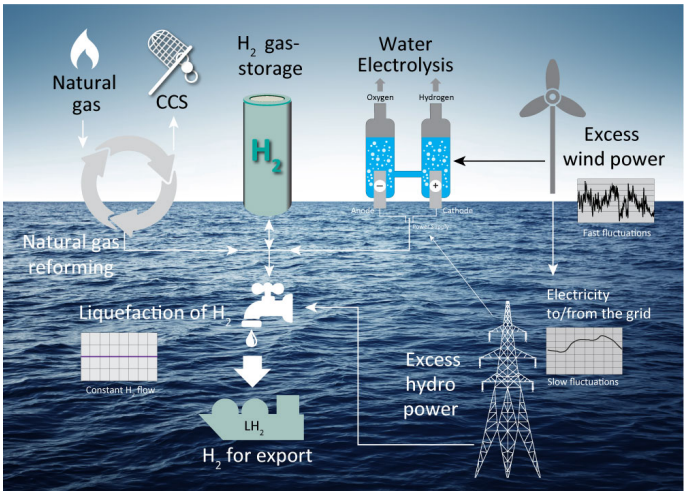

Figure 1.1: Illustration of the process of producing liquid hydrogen with low CO_2 emmision.

Today, most of the hydrogen is produced form either natural gas,

oil or coal. Producing hydrogen form these sources will produce CO_2. However, hydrogen may be considered a clean energy carrier if Carbon Capture and Storage (CCS) is performed. Figure 1.1 [5] illustrates the components needed for producing liquid hydrogen with a minimum of CO_2 produced. Producing hydrogen from fossil fuels while preforming CCS, enables low emission utilization of fossil energy resources.

1.2 Hydrogen and Hydrogen Liquefaction

Properties of Hydrogen

We have now established that hydrogen may be an important component in a low emission future. Before considering hydrogen as an energy carrier, we need to study some fundamental properties of hydrogen.

Hydrogen is the first element in the periodic table with the atomic number 1. It has been estimated that hydrogen makes up 75% of the mass of the universe [6], which makes hydrogen the most common element in the universe. Hydrogen is found as an important component in proton-proton reaction which is the main source of energy radiated form the sun. Most of the hydrogen on earth occurs in combination with oxygen in water. Hydrogen is also found in organic compounds.

The word *hydrogen* originates from the Greek word hydrogenium ($\upsilon\delta\omega\rho\gamma\epsilon\nu\nu\epsilon\iota\nu$) and is composed of two words: *hydro*($\upsilon\delta\omega\rho$), which means *water* and *genium* ($\gamma\epsilon\nu\nu\epsilon\iota\nu$), which means *to give birth* [6], as it in combustion with oxygen produces water. It was given this name in 1787 by the French scientist *Antoine Lavoisier*(1743-1794). Before, hydrogen was known as *inflamable air*, as it easily catches fire.

The most common isotope of hydrogen is called *protium*. 99.985 % of all hydrogen in the universe is protium. This isotope is composed of one proton and one electron, and has an atomic mass of 1.0078u.

There are two other hydrogen isotopes. *Deuterium* is the second most common, and is composed of one electron, one proton and one neutron, and has an atomic mass of 2.0140u. The last hydrogen isotope is *tritium*, which is composed of one electron, one proton and two neutrons with an atomic mass of 3.01605u. As the occurrence of deuterium and tritium are small compared to protium, this study will treat hydrogen as a fluid of pure protium.

As mentioned, protium, or hydrogen, is composed of one electron and one proton. Protons and electrons are members of the group of quantum particles called fermions. Fermions are characterized by a spin of 1/2 which can either be directed upwards $|\uparrow\rangle$, or downwards $|\downarrow\rangle$ [7]. When two hydrogen atoms come together and form a H_2 molecule, the spin of the protons in the nucleus will either be directed in the same direction or the opposite direction. Spin directed in the same direction, results in three quantum states, which we can write as $|\uparrow\uparrow\rangle$, $|\downarrow\downarrow\rangle$ and $1/\sqrt{2}(|\uparrow\downarrow\rangle + |\downarrow\uparrow\rangle)$. These three quantum states are degenerated, which means that they correspond to the same energy state. H_2 molecules in this quantum states are called orthohydrogen. The other option for the H_2 molecule, is to couple up with spins directed in opposite directions. This corresponds to a fourth quantum state given by $1/\sqrt{2}(|\uparrow\downarrow\rangle - |\downarrow\uparrow\rangle)$. This state is called parahydrogen. Figure 1.2 illustrates the spin directions of para- and orthohydrogen.

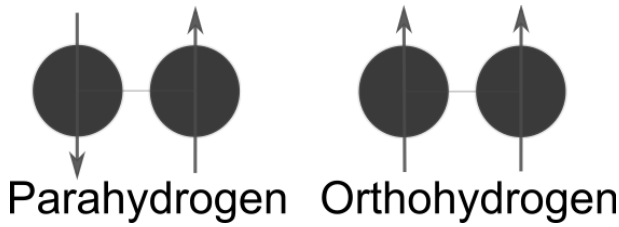

Figure 1.2: Para- and orthohydrogen.

With its spin pointing in the same direction, orthohydrogen has

the highest eigen energy. At ambient conditions 75% of the hydrogen will be orthohydrogen and 25% is parahydrogen [8], as there is enough thermal energy in the system to have an equal distribution between the four quantum states. When the temperature is lowered, the thermal energy of the system will decrease, and the amount of orthohydrogen will decrease, and parahydrogen increase. At about 77K, there will be only 50% orthohydrogen [9], and at the critical point, the equilibrium composition is almost pure parahydrogen.

Thus, when cooling hydrogen, there will be a spin-isomer conversion reaction taking place given by

$$\mathrm{H}_2^{\mathrm{ortho}} \rightleftharpoons \mathrm{H}_2^{\mathrm{para}}. \tag{1.1}$$

As the energy of orthohydrogen is higher than the energy of parahydrogen, energy will be released in this reaction [10]. When the temperature is lowered, the ortho-to-para conversion will occur spontaneous in order to maintain an equilibrium concentration. This reaction is exothermic, and generates a heat of about 1.623kJ/mol. The latent heat of hydrogen evaporation is 0.891kJ/mol. This means that if there is already liquid hydrogen in the system, there will be spontaneous evaporation of the liquid hydrogen. This phenomena is called *boil off* [10].

Hydrogen Liquefaction

From a gravimetric point of view, there is a large amount of energy "hidden" in hydrogen, but due to its low density, the energy density of hydrogen is rather low compared to other energy carriers such as gasoline and state of the art batteries. Increasing the energy density of hydrogen can either be done by compression or by liquefaction. In a study by Berstad et al. it was found that liquid hydrogen contains about four times more energy per volume compared to compressed

hydrogen at 250 bar, and almost three times as much compared to hydrogen compressed at 350 bar [11].

Today, some of the largest technological challenges concern storage and transportation of hydrogen. Using liquid hydrogen (instead of compressed), will reduce necessary storage and transportation volume, which is of particular interest for large scale transportation of hydrogen from remote production location to filling stations in cities. Thus, the energy density of hydrogen is a significant factor for the overall hydrogen economy.

A typical modern hydrogen liquefaction plant uses a four-step process [10, 12, 15].

Step 1: Pre-compression of the hydrogen gas (this is not always required).

Step 2: Pre-cooling of the hydrogen gas to about 80K.

Step 3: Cryogenic cooling of the hydrogen gas to about 20-30K.

Step 4: Final expansion and liquefaction of the hydrogen.

Current hydrogen liquefaction technologies have a high power consumption [11] and the cryogenic part of the heat exchanger is responsible for a large amount of the exergy destruction in the liquefaction process [12]. Reducing the lost work by making more energy efficient heat exchangers is necessary in order to make hydrogen a competitive and attractive energy carrier.

1.3 Entropy Production and Second Law efficiency

We now need some tools to understand energy efficient heat exchanger design. By energy efficiency, we refer to the second law efficiency.

We know from the second law of thermodynamics that any real, or irreversible, process is producing entropy. From experience we know that two processes doing the same task, may not produce the same amount of entropy. This means that there exists a path which produces a minimum of entropy [13].

The energy efficiency of a process may be measured by the *Second Law Efficiency*. The second law efficiency is related to second law of thermodynamics, which says that the quality of the energy is reduced in all real processes due to irreversibility. An example of this is heat which has lower energy quality than work. This means that you can convert 1 Joule of work into heat, but if you have 1 Joule of heat, you will not retrieve 1 Joule of work.

The second law efficiency (η_{II}) takes into account the quality of different energy sources/sinks by using the work-equivalent energy form of all inputs and outputs in the process. This enables us to calculate the work produced or consumed w by the process. For an ideal process (completely reversible process), the work produced or consumed is w_{ideal}.

For a work consuming process ($w > 0$), the ideal work is the minimum amount of work possible to consume. For these processes the second law efficiency takes the form

$$\eta_{II} = \frac{w_{ideal}}{w}. \tag{1.2}$$

Thus, the second law efficiency is a number between zero and one that reflects the degree of irreversibility in a process. The difference between the ideal work and the real work is called the *lost work* w_{lost}. The lost work is related to the entropy production through the Gouy-Stodola theorem [14] given by

$$w_{lost} = w - w_{ideal} = T_0 \left(\frac{dS}{dt} \right)_{irr}. \tag{1.3}$$

Here T_0 is the temperature of the environment, S is the entropy and the subscript *irr* stands for irreversible. This theorem shows that irreversibility is what causes the deviation between real work and ideal work. Derivations of this theorem for general processes can be found in for example Bejans book on *Entropy Generation Minimization* [14].

This relation can be used to derive a direct relation between the efficiency of a process and the entropy production given by

$$\eta_{II} = \frac{w_{ideal}}{w_{ideal} + T_0 \left(\frac{dS}{dt}\right)_{irr}}. \tag{1.4}$$

From equation (1.4) we note that maximizing the second law efficiency is equivalent to minimizing the entropy production, if the ideal work is fixed. Even if the ideal work is not fixed, the energy efficiency and the entropy production are still related through the Gouy-Stodola theorem in equation (1.3), which states that the irreversibility of the system is the main source of energy inefficiency. This is why we are studying the state of minimum entropy production in hydrogen liquefaction.

Entropy production minimization is a field of irreversible thermodynamics which has been studied by many authors over the last couple of decades [16–30]. In this field, there are two important theorems which are used as design criterias in chemical reactors and heat exchangers. The first theorem is equipartition of forces (EoF) [20–22], and the second equipartition of entropy production (EoEP) [23–25]. The equipartition theorems say that the state of minimum entropy production is characterized by constant thermodynamic forces (EoF) and constant local entropy production (EoEP).

The derivation of the equipartition theorems requires that all thermodynamic forces of the system can be controlled. This is not necessarily the case in real systems. In 2004, Eivind Johannessen [13] wrote his doctor thesis on the state of minimum entropy production

in an optimally controlled system. This thesis is based on his work on entropy production minimization on systems with too few control variables.

1.4 Aim and Structure of this thesis

In this study, we will look deeper into the cryogenic step of the hydrogen liquefaction process. We will study energy efficient heat exchanger design by using tools form irreversible thermodynamics and optimal control theory. The optimized hydrogen heat exchanger will be compared to results given in literature.

There are two properties of the hydrogen liquefier which distinguish it from earlier studies on entropy production minimization. 1. We are not working with a chemical reaction, but a spin-isomer conversion reaction. 2. We use a real equation of state. In earlier studies, only the ideal gas equation of state has been considered.

Our aim is to investigate the path of minimum entropy production in a hydrogen liquefier at low temperatures and map its properties. In the long run, we hope to contribute to more energy efficient heat exchanger design which will lead to less CO_2 emission to the atmosphere.

The thesis is structured in the following way:

Chapter 2 - Theory This chapter introduces the theory and the models used and is composed of four parts: The heat exchanger, the balance equations, irreversible thermodynamics and the equation of state.

The first part introduce our heat exchanger and its properties together with necessary simplifications. The second part concerns the governing equations of the system, which are necessary to establish before we can go on to the third part, which overlooks

the thermodynamics of the system and introduced the entropy production equations. In the last part of the theory, we will talk about the real gas equation of state used in this study.

Chapter 3 - Method In this chapter a short review of optimal control theory will be presented and we will formulate the optimal control problem for the hydrogen heat exchanger.

Chapter 4 - Cases In this chapter, we will introduce the cases the we are going to study.

Chapter 5 - Results and Discussion This chapter is divided in two parts. First, we will discuss the consistency of the system. Then, we will look at the results of the optimizations and discuss properties of the optimal hydrogen heat exchanger.

Chapter 6 - Conclusion In the last chapter, there will be a summary of the main findings in this study.

Chapter 2

Theory

2.1 The Plate Fin Heat Exchanger

In this thesis, we want to model a hydrogen heat exchanger which is as close as possible to a real heat exchanger used in industry. *Plate Fin Heat Exchangers* are widely used in cryogenic applications as their finned geometry results in a large heat exchange area to volume ratio which enables heat transfer at small temperature differences. Modern hydrogen liquefaction plants use plate fin heat exchangers for efficient cooling of the hydrogen gas [10, 12].

A plate fin heat exchanger consists of alternating streams of hot and cold fluids. This is illustrated in Figure 2.1 which shows parts of a plate fin heat exchanger. The blue chambers contain a cold fluid, and the red chambers contain a hot fluid.

By neglecting boundary effects, the heat exchanger can be represented by considering n_r different hot and cold streams, which together form one sequence of the heat exchanger. The sequence is repeated N times. This results in a total $n = n_r N$ streams which forms our

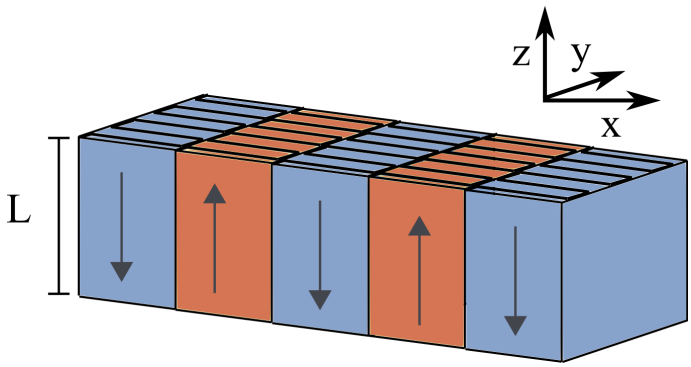

Figure 2.1: Illustration of a plate fin heat exchanger with alternating hot (read chambers) and cold (blue chambers) streams. The arrows inside the chambers indicates the flow direction of the streams.

plate fin heat exchanger. Some of the layers contain catalyst pellets as illustrated in Figure 2.2. In our case, these are the hot streams, where the ortho-para conversion reaction from equation (1.1) is taking place. The cold streams contain a cooling medium, which can for example be hydrogen or a mixture of neon and helium (nelium) [12].

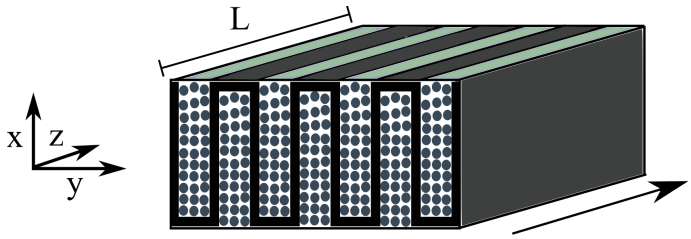

Figure 2.2: Illustration of one chamber filled with catalyst pellets. The arrow indicate the flow direction of the hydrogen gas.

In the optimization we need to simplify the system, as optimizing several sequences of hot and cold streams will be a time consuming

and complicated procedure. We are therefore only look at one chamber filled with catalyst pellets. Inside the chamber the hydrogen isomer reaction (1.1) is taking place. For simplicity, we will illustrate this chamber as a cylindrical heat exchanger, as illustrated in figure 2.3.

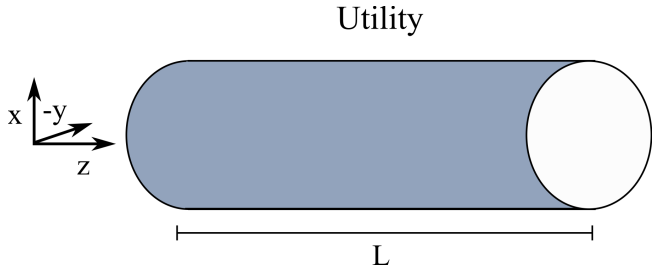

Figure 2.3: Simplified illustration of one layer of the heat exchanger.

In our model, the cold streams from Figure 2.1 are replaced by a cooling medium completely surrounding the heat exchanger. We call this cooling medium the *Utility*.

2.2 The Balance Equations

We are working with a heat exchanger containing hydrogen. We want to optimize the energy consumption of the heat exchanger while the hydrogen spin-isomer reaction (1.1) is taking place. When modeling this system, we need the balance equations. The balance equations describe the evolution of the state variables. In this system, there are three state variables: the temperature (T) of the H_2 gas inside the heat exchanger, the pressure (P) inside the heat exchanger, and the chemical composition (ξ). We also have one control variable. This is the temperature outside the heat exchanger. We call this the temperature of the utility (T_a).

We want to model a system of 2 components and 1 reactions. The two components being orthohydrogen and parahydrogen, and the reaction being the spin-isomer reaction (1.1). The simplified model described in section 2.1 is sketched in Figure 2.4.

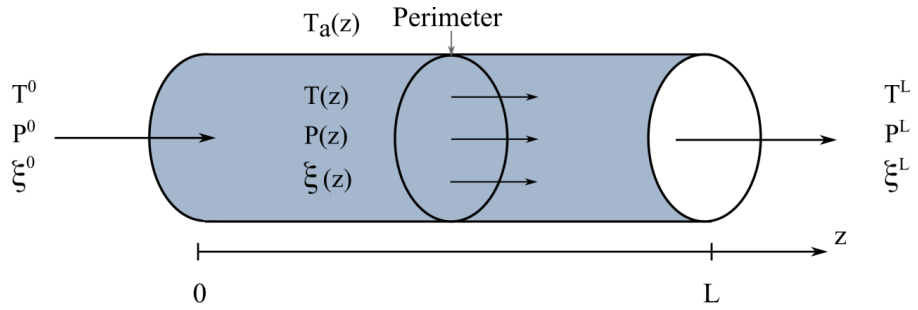

Figure 2.4: Simplified illustration of the heat exchanger.

The reaction is taking place at the catalyst surface. We choose a reference component, A, and arrange the reaction in the following way

$$0 = -A + \sum_{i,i\neq A} \nu_i B_i, \tag{2.1}$$

Here B_i is component i, and ν_i is the stoichiometric coefficient of component i.

We now define the conversion of the reaction as

$$\xi_{=} \frac{\text{moles of A consumed by the reaction}}{\text{moles of A at inlet}}. \tag{2.2}$$

The conversion is a unitless quantity which describes how much of a reactant has reacted.

Further, we define the molar flow rate by

$$F_i = F_A^0 \big[\theta_i + (\nu_i \xi)\big]. \tag{2.3}$$

The flow rate describes how fast the chemical components "travel" through the system, and it has dimension *mole/s*. The superscript 0 means values at inlet, subscript A, refers to the reference component A and $\theta_i = \frac{F_i^0}{F_A^0}$ and $\theta_T = \frac{F_T^0}{F_A^0}$.

As mentioned, there are three state variables in this system, namely the temperature T, the pressure P and the conversion ξ. The differential equations describing the evolution of these three quantities are the energy-, momentum and mass-balance equations. These equations are described in text books on chemical reaction engineering such as Fogler [31].

The derivation of the *energy balance equation* starts with the first law of thermodynamics [31]

$$dU = \delta Q - \delta W \tag{2.4}$$

Where U is the total energy of the system, δQ is the heat added to the system and δW it the work done by the system on the surroundings.

If we differentiate this equation with respect to time, we get the following equation

$$\frac{dU_{system}}{dt} = \dot{Q} - \dot{W} + \sum_{i=1}^{n}(F_i e_i)|_{inlet} - \sum_{i=1}^{n}(F_i e_i)|_{outlet}. \tag{2.5}$$

Here e_i is the molar energy of component i, and the $\cdot$ over the letters indicate time derivatives.

The work term can be written as

$$\dot{W} = -\sum_{i=1}^{n} F_i P\tilde{V}_i|_{inlet} + \sum_{i=1}^{n} F_i P\tilde{V}|_{outlet} + \dot{W}_s \tag{2.6}$$

where $\tilde{V}_i$ is the specific molar volume of component i, P is the pressure and $\dot{W}_s$ is the shaft work.

In our system, we will assume steady state, which means that $\frac{dU_{system}}{dt} = 0$. We also assume that $\dot{W}_s = 0$ as there is no stirrer. By using the relation $h_i = e_i + P_i\tilde{V}_i$, where h_i is the molar enthalpy of component i, and by considering a small volume dV of the heat exchanger, equation (2.5) simplifies to

$$\begin{aligned} &\Delta\dot{Q} + \sum_{i=1}^{n}(F_i h_i)|_V - \sum_{i=1}^{n}(F_i h_i)|_{V+dV} \\ &= \Delta\dot{Q} - \sum_{i=1}^{n}\frac{d(F_i h_i)}{dV} = 0. \end{aligned} \tag{2.7}$$

$\Delta\dot{Q}$ is the heat flow to the heat exchanger from the surroundings which is equal to the heat flux J_q through the heat exchanger walls times a geometrical factor. The other part of this expression can be simplified by using the chain rule

$$\begin{aligned} \sum_{i=1}^{n}\frac{d(F_i h_i)}{dV} &= \sum_{i=1}^{n}\frac{dF_i}{dV}h_i + \sum_{i=1}^{n}F_i\frac{dh_i}{dV} \\ &= r(-\Delta_r H) + \sum_{i=1}^{n}F_i C_{p,i}\frac{dT}{dV} + \left(\frac{\partial H_i}{\partial P}\right)_{T,F_i}\frac{dP}{dV}. \end{aligned} \tag{2.8}$$

Here we used that

$$\sum_{i=1}^{n}\frac{dF_i}{dV}h_i = \sum_{i=1}^{n}\nu_i h_i(-r) = r(-\Delta_r H) \tag{2.9}$$

and

$$\sum_{i=1}^{n} F_i \frac{dh_i(T,P)}{dV} = \sum_{i=1}^{n} F_i C_{p,i} \frac{dT}{dV} + \left(\frac{\partial H_i}{\partial P}\right)_{T,F_i} \frac{dP}{dV}. \tag{2.10}$$

Here H_i is the enthalpy of component i and $\Delta_r H$ is the enthalpy of the reaction.

By combining equation (2.7) and equation (2.8), and rearranging the expression, we get the following energy balance equation for the system

$$\frac{dT}{dz} = \frac{\mathcal{P} J_q + \Omega[r(-\Delta_r H)] - \left(\frac{\partial H_i}{\partial P}\right)_{T,F_i} \frac{dP}{dz}}{\sum_{i=1}^{n} F_i C_{p,i}}. \tag{2.11}$$

Here $\mathcal{P}$ is the perimeter of the heat exchanger, Ω the cross sectional area, r and is the reaction rate and $C_{p,i}$ the specific heat of component i.

The *momentum balance* equation relates the pressure drop (dP/dz) to the fluid velocity (v). For a fully developed flow, the pressure drop can be modeled by Hicks equation [26]

$$\frac{dP}{dz} = f\rho v^2 / D_p. \tag{2.12}$$

Where D_p is the diameter of the catalyst pellets, and f is the friction factor. The friction factor if given by

$$f = 6.8 \frac{(1-\epsilon)^{1.2}}{\epsilon^3 Re_p^{0.2}}. \tag{2.13}$$

Here $Re_p = D_p v L \rho / \mu$, where μ is the viscosity of the fluid and L is the length of the heat exchanger. ϵ is the catalyst bed void fraction.

The last balance equation we want to study describes the evolution of the conversion (the amount of reacted reactant) through the heat exchanger and is called the *mass balance equation*.

The mass balance (or mole balance) is given by [31]

$$\sum_{i=1}^{n} \frac{dF_i}{dV} = r. \tag{2.14}$$

By using equation (2.3), we can express the mass balance in terms of the conversion. This results in the following balance equation relating the change in conversion to the reaction rate.

$$\frac{d\xi}{dz} = \frac{\Omega}{F_A^0} r. \tag{2.15}$$

More details on the calculations of the balance equations can be found in the book by Fogler on chemical reactions [31].

2.3 Non-Equilibrium Thermodynamics

Now that we have characterized our hydrogen heat exchanger, the next step is to analyze the efficiency of the liquefaction system. This can be done by using tools from non-equilibrium thermodynamics.

Non-equilibrium thermodynamics is a branch of thermodynamics describing transport properties in systems which are not in a global equilibrium. The field was established in 1931 when Lars Onsager published his famous Onsager relations. Onsager reformulated the second law of thermodynamics as a product sum of the so-called conjugate fluxes (J_i) and forces (X_i) of the system. This resulted in the following equation for the local entropy production

$$\sigma = \sum_{i=1}^{n} J_i X_i \geq 0. \tag{2.16}$$

Here, n is the number of conjugate fluxes and forces. Non-equilibrium thermodynamics (also called irreversible thermodynamics) describe how different transport properties in a system are influenced by each other. In irreversible thermodynamics it is common to assume a linear relation between the fluxes and forces given by

$$J_i = \sum_{j=1}^{n} L_{ij} X_j \qquad \text{, for} \quad j = 1, ..., n. \tag{2.17}$$

Here, the L_{ij} are conductivity coefficients. More details about the Onsager relation and conjugate fluxes and forces can be fond in the book by Kjestrup et al. on Non-Equilibrium Thermodynamics [39].

2.3.1 Entropy Production

As mentioned in the introduction, the lost work is related to the entropy production through the Gouy-Stodola theorem [14]. This is why we are interested in studying entropy production minimization.

The entropy production can be found in two ways:

- Total entropy balance over the system
- Local entropy balace over the system

The two methods for obtaining the entropy production are equivalent.

The total entropy balance over the heat exchanger is given by the entropy going out of the system minus entropy coming in. As shown in figure 2.5, entropy is flowing out through the heat exchanger outlet,

and flowing in through the inlet. There will also be entropy "flowing" though the heat exchanger walls due to heat transfer with the utility. This is what in figure 2.5 is called S_{boundary}.

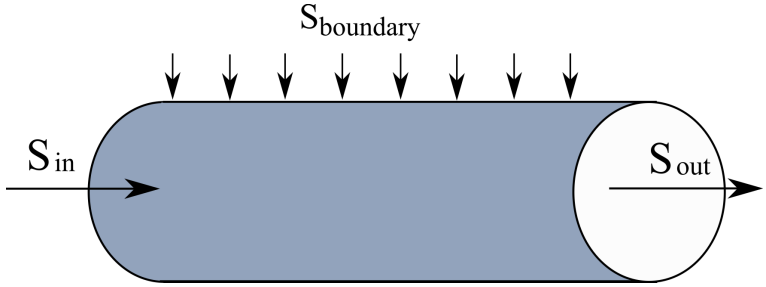

Figure 2.5: The figure shows where entropy enters and leavs the system.

With this in mind, we can formulate an equation describing the total entropy produced in the system

$$(\frac{dS}{dt})_{irr} = F_{out}s_{out} - F_{in}s_{in} - \int_0^L \mathcal{P}\frac{J_q}{T_a}dz. \tag{2.18}$$

Here L is the length of the heat exchanger and T_a is the temperature of the utility. s_{in} and s_{out} are molar entropies at outlet and inlet respectively and F_{in} and F_{out} are the molar flow rate, also evaluated at the inlet and the outlet of the heat exchanger. The last term in the equation represents the heat transferred form the utility. J_q is the heat flux through the walls, given by

$$J_q = U(T - T_a), \tag{2.19}$$

where U is the overall heat transfer coefficient. This coefficient is system specific. In this study, it is regarded as a constant.

By using the chain rule the expression for the total entropy production given in equation (2.18) can be written as

$$(\frac{dS}{dt})_{irr} = \int_0^L (\frac{d(F \cdot s)}{dz} - \mathcal{P}\frac{J_q}{T_a})dz = \int_0^L \sigma dz. \tag{2.20}$$

Here σ is the *local* entropy production. We can use this expression to derive the local entropy balance over the system.

As mentioned earlier, there are three state variables of the system, namely temperature (T), pressure (P) and the chemical composition (here represented with the flow rate F_i). We therefore rewrite the expression $d(FS)/dz$ as derivatives of the three variables of the system and we get a new expression for the local entropy production given by

$$\sigma = \frac{dT}{dz}\left(\frac{\partial(Fs)}{\partial T}\right)_{F_i,P} + \frac{dP}{dz}\left(\frac{\partial(Fs)}{\partial P}\right)_{T,F_i} + \sum_{i=0}^{n} \frac{dF_i}{dz}\left(\frac{\partial(Fs)}{\partial F_i}\right)_{P,T} - \mathcal{P}\frac{J_q}{T_a}. \tag{2.21}$$

We assume ideal mixing, which allows us to write FS in the following way

$$Fs = \sum_{i=1}^{n} \left[s_i F_i - F_i R \ln\left(\frac{P}{P_0} x_i\right) \right], \tag{2.22}$$

where R is the gas constant and P_0 is a reference pressure. By using this expression, we can now formulate the partial derivatives in equation (2.21) as,

$$\begin{aligned} \frac{\partial(Fs)}{\partial T} &= \sum_{i=1}^{n} F_i \frac{\partial s_i}{\partial T} = \frac{1}{T} \sum_{i=1}^{n} F_i C_{p,i} \\ \frac{\partial(Fs)}{\partial P} &= -\frac{R}{P} \sum_{i=1}^{n} F_i = -\frac{\Omega v}{T} \\ \frac{\partial(Fs)}{\partial F_i} &= s_i - R \ln\left(\frac{P}{P_0} x_i\right) \end{aligned} \tag{2.23}$$

By inserting these equations back into equation (2.21) combined with the balance equations given in section 2.2, we obtain a new expression for the local entropy production

$$\sigma = \Omega r\big(-\frac{\Delta_r G}{T}\big) + \mathcal{P} J_q \Delta\big(\frac{1}{T}\big) + \Omega v\big(-\frac{1}{T}\frac{dP}{dz}\big). \tag{2.24}$$

Table 2.1: Flux - force relations in the local entropy production.

Description	Symbol	Entropy Production	Flux	Driving Force
Heat Transfer	σ_q	$\mathcal{P} J_q \Delta\big(\frac{1}{T}\big)$	J_q	$\Delta\frac{1}{T}$
Frictional Flow	σ_p	$\Omega v\big(-\frac{1}{T}\frac{dP}{dz}\big)$	v	$-\frac{1}{T}\frac{dP}{dz}$
Reaction	σ_{rx}	$\Omega r\big(-\frac{\Delta_r G}{T}\big)$	r	$-\frac{\Delta_r G}{T}$

We can recognize this expression as a product sum of conjugate fluxes and forces on the same form as equation (2.16). In this heat exchanger there are three phenomenas that produce entropy: The reactions, the heat transfer through the walls, and the frictional flow (pressure drop). Table 2.1 shows the three contributions to the entropy production, as well as all the conjugate fluxes and forces. For more details on flux - force relations see the book of Kjelstrup et al [39].

2.3.2 Highway in State Space and Equipartition Theorems

In literature, there are two theorems characterizing the state of minimum entropy production. These are the equipartition theorems. The equipartition theorems are used as design criteria for chemical reactors and heat exchangers when some assumptions are fulfilled [13, 20, 21, 25, 39].

The theorem of equipartition of entropy production (EoEP) says that the state of minimum entropy production is characterized by a constant local entropy production. The theorem is based on two assumptions.

1 First we need to assume that there are enough control variables to control all forces independently and without constraints on their values. In a system of n state variables, and m control variables, there has to be at least $m \geq n$ control variables.

2 Secondly, we need to assume linear flux-force relation, as given in equation (2.17).

The theorem of equipartition of forces (EoF) is similar to the theorem of equipartition of entropy production, only here, the thermodynamic driving forces are constant through the system. For this theorem to apply, we need to do some further assumptions. I will not go into details about the assumption for EoF here. For more details on the theorems and derivations see reference [25, 28].

In the problem studied in this thesis, the first assumption is not fulfilled, as there are three state variables in the system (temperature, pressure and chemical composition), and only one control variable. Thus, the equipartition theorems do not apply. Johannessen at al [28] proposed a hypothesis for the state of minimum entropy production in a system where there are less control variables than state variables.

> EoEP, but also EoF are good approximations to the state of minimum entropy production in the parts of an optimally controlled system, that have sufficient freedom. [28]

According to this hypothesis, EoEP and EoF are states which are close to the state of minimum entropy production in a system with less

control variables than state variables, if the system has sufficient freedom. A system with enough control variables have in general sufficient freedom. A system with too few control variables does not in general have sufficient freedom in the whole system. There will be restrictions to the solution such as boundary conditions and compromise between dissipative phenomena [28].

In 2005, Eivind Johannessen studied optimal reactor design in plug flow reactors, similar to the heat exchanger we are studying here [28]. In this study, he observed a highway in state space. The highway is the most energy efficient path in state space, and it is characterized by approximately constant driving forces and entropy production. The discovery of the highway made it possible to make a general model for reactor/heat exchanger design, as it turns out that the optimal path of a system will in the central regions of a reactor/heat exchanger follow the same path, independently of temperature and pressure boundary conditions.

2.4 Equation of State

Equations of state are equations what relate the state variables of a system together. The most know equation of state is the *ideal gas law* given by

$$P = \rho RT. \tag{2.25}$$

This law relates the three state variables: pressure (P), density (ρ) and temperature (T). R is the gas constant. As one could guess from the name, this law only applies to systems of ideal gases. An ideal gas is a gas where all the particles are regarded as point particles, only interacting in no elastic collisions with the walls.

For many application, this is not a sufficient description of the system, as the particles interact all the time. Therefore, there has

been developed several models for describing real fluid behavior. One of these models is the multiparameter equation of state.

2.4.1 Multiparameter Equation of State

The most accurate equation of state used in thermodynamic molding of hydrogen is the multiparameter equation of state based on the *Helmholtz energy*, $a = a(T, \rho)$. This is a fundamental equation of state with temperature (T) and density (ρ) as independent variables. The equation of state can be used to model both the liquid and the gaseous state. The advantage with a Helmholtz energy based formulation is that when $a(T, \rho)$ is known, it is possible to calculate all thermodynamic properties by combination of derivatives of a with respect to T and ρ [43]. The Helmholtz energy (or Helmholtz equation) is normally formulated in reduced (dimensionless) form

$$\alpha = \frac{a(T, \rho)}{RT}, \tag{2.26}$$

where $\tau = T_c/T$ and $\delta = \rho/\rho_c$, and T_c and ρ_c are the critical temperature and density respectively. It is convenient to split the equation into two terms, one representing the ideal gas behavior and one representing the residual behavior of the real gas

$$\alpha(\tau, \delta) = \frac{a^0(T, \rho) + a^r(T, \rho)}{RT} = \alpha^0(\tau, \rho) + \alpha^r(\tau, \rho). \tag{2.27}$$

Here $\alpha^0(\tau, \delta)$ models the ideal gas behavior, and $\alpha^r(\tau, \delta)$ models the residual behavior of the real fluid.

Ideal Gas Properties of Helmholtz energy

The Helmholtz energy of an ideal gas is given in most text books on thermodynamics [32, 37, 43], and is commonly formulated as

$$a^0 = h^0 - RT - Ts^0. \tag{2.28}$$

h^0 and s^0 are ideal gas molar enthalpy and entropy respectively. The enthalpy and entropy are normally formulated the following way

$$\begin{aligned} h^0 &= h_0^0 + \int_{T_0}^{T} c_p^0 dT \\ s^0 &= s_0^0 + \int_{T_0}^{T} \frac{c_p^0}{T} dT - R\ln\left(\frac{\rho T}{\rho_0 T_0}\right). \end{aligned} \tag{2.29}$$

Here h_0^0 and s_0^0 are reference molar enthalpy and entropy, T_0 and P_0 are arbitrary constants. ρ_0 is the ideal gas density at T_0 and P_0 [40,43]. Combining these equations, we get the ideal gas Helmholtz energy

$$a^0 = h_0^0 + \int_{T_0}^{T} c_p^0 dT - RT - T\left[s_0^0 + \int_{T_0}^{T} \frac{c_p^0}{T} dT - R\ln\left(\frac{\rho T}{\rho_0 T_0}\right)\right], \tag{2.30}$$

which can be written in reduced form as

$$\alpha^0 = \frac{h_0^0 \tau}{RT_c} - \frac{s_0^0}{R} - 1 + \ln\frac{\delta\tau_0}{\delta_0\tau} - \frac{\tau}{R}\int_{\tau_0}^{\tau} \frac{c_p^0}{\tau^2} d\tau + \frac{1}{R}\int_{\tau_0}^{\tau} \frac{c_p^0}{\tau} d\tau, \tag{2.31}$$

with $\delta_0 = \rho_0/\rho_c$ and $\tau_0 = T_c/T_0$. By computing the integrals, the equation simplifies, and we end up with the following equation for the ideal gas reduced Helmholtz energy

$$\alpha^0(\delta,\tau) = \ln\delta + 1.5\ln\tau + a_1 + a_2\tau + \sum_{k=3}^{N} a_k \ln[1 - e^{b_k\tau}]. \tag{2.32}$$

The parameters a_k and b_k are given by Leachman et al. [8].

Real Fluid Properties

The residual contribution to the Helmholtz energy models the properties of the real fluid not covered by the ideal gas. This is all kinds of molecular interactions. The behavior of real fluids is complex. In contrast to ideal gas, real fluid properties are modeled by using empirical models, which are only loosely supported by theoretical considerations [40]. In 2009, Leachman et al. [8] did a study on thermodynamic properties of hydrogen, and they proposed an equation for the residual contribution to the Helmholtz energy

$$\begin{aligned}\alpha^r(\delta,\tau) = &\sum_{i=1}^{l} N_i \tau^{t_i} \delta^{d_i} + \sum_{i=l+1}^{m} N_i \tau^{t_i} \delta^{d_i} e^{-\delta^{p_i}} \\ &+ \sum_{i=m+1}^{n} N_i \tau^{t_i} \delta^{d_i} e^{\phi_i(\delta - D_i)^2} e^{\beta_i(\tau-\gamma_i)^2}.\end{aligned} \tag{2.33}$$

Here, $l = 7, m = 9$, $n = 14$ and $N_i, d_i, t_i, p_i, \phi_i, D_i, \beta_i$ and γ_i are constants, given by Leachman et al. [8]. More information on the multiparameter equation of state can be found in the book on Multiparameter Equation of State by Span [43], in the article by Leachmann et al. [8] and in the article by Lemmon et al. [40].

This is the equation of state used in this study. All parameters and critical values can be found in the article of Leachmann et al. [8], and the equations for entropy, enthalpy and heat capacity is given in Appendix A.1.

In this chapter, we have covered the theory necessary for this thesis. The first part of this chapter concerned the geometry and simplifications in our plate fin heat exchanger. It is important to understand the system that we are studying before we can understand its behavior. The second part concerned the balance equations, which are impor-

tant equations describing the evolution of our state variables. They are used in both the derivation of the entropy production (see section 2.3) and in the optimal controlled problem, which we will describe in detail in the next chapter. The third part of this chapter consider the entropy production. As the title of this thesis may imply, the core of this study is to understand mechanisms for entropy production in the hydrogen liquefier. The entropy production equation introduced in this section will be used in the formulation of the optimal controlled problem. The final part of this chapter concerned the equation of state, which is the fundamental equation of our system.

Chapter 3

Method

3.1 Optimal Control Theory

The goal of this study is to find optimal cooling strategies for the cryogenic step of the hydrogen liquefaction process. In this case, the optimal cooling strategies refers to the most energy efficient cooling of the system. This is equivalent to minimizing the entropy production [27–29, 39]. As the temperature of the utility is the only variable that we control, the task is to find the $T_a(z)$ that gives the minimum entropy production.

In an unconstrained system, the problem would simply be to solve the extremal condition

$$\frac{\partial \phi}{\partial x_i} = 0 \qquad \text{, for} \quad i = 1, ..., n. \tag{3.1}$$

where ϕ is the function that we want to minimize and x_i are the variables of the system and n is the number of variables. In physical systems, there are often constraints on the system that prevent the variables from varying freely. In these constrained systems, equation

(3.1) can no longer be used to find the extremum values. In those cases, we need to introduce optimal control theory, which is a method using Lagrange multipliers to solve constrained optimization problems. In 2004, Eivind Johannessen [29] studied a SO_2 reaction in a plug flow reactor. He did a numerical optimization of the entropy production in the system. During this study, Eivind implemented an optimization algorithm that is specially designed for entropy production minimization in chemical reactors and heat exchangers. As we will be using a similar method, we will here give a summary of this optimization process.

In optimal control theory there are two classes of variables: *state variables* $\mathbf{x}(z)$ and *control variables* $\mathbf{u}(z)$. The state variables $\mathbf{x}(z)$ with $x = \{x_1, ..., x_N\}$, is a set of variables, representing a trajectory through the N-dimensional phase space $\mathbb{P}$ of the underlying system, where N is the number of state variables in the system. In other words, the state variables specify the system. The state variables may be constrained. A constrained variable does not vary freely but are subject to some restrictions. In the optimal controlled problem that we study here, the constraints f_k are formulated as a set of differential equations, describing the evolution of the system

$$f_k = \frac{\partial x_k(z)}{dz} \qquad \text{, for} \quad k = 1, ..., p. \tag{3.2}$$

where p is the number of constraints.

The control variables $\mathbf{u}(z)$, with $u = \{u_1, ..., u_r\}$, is the set of variables that control the system. Here, r is the number of control variables in the system. A control variable could for example be an external force acting on a system. The optimal controlled problem consists of finding the optimal controls.

In order to find these optimal controls, we need to construct a

Hamiltonian given by

$$H(\mathbf{x}(z), u(z), \lambda(z)) = \phi(\mathbf{x}(z), u(z)) + \sum_{i=1}^{p} \lambda_i f_i, \tag{3.3}$$

where ϕ is the function that we want to minimize and λ_k are the Lagrange multipliers.

The optimal path is found by solving the canonical equations, given by

$$\begin{aligned} \frac{x_k(z)}{dz} &= \frac{\partial H}{\partial \lambda_k} \\ \frac{\lambda_k(z)}{dz} &= -\frac{\partial H}{\partial x_k}, \end{aligned} \tag{3.4}$$

for $k = 1, ..., p$. The final condition needed to solve the problem is given by

$$\frac{\partial H^*}{\partial \mathbf{u}^*} = 0. \tag{3.5}$$

Here H^* and $\mathbf{u}^*$ is the optimal Hamiltonian and optimal control vector respectively. This condition needs to be satisfied at every position z.

3.1.1 The Optimal Controlled Hydrogen Heat Exchanger

Now we can formulate the optimal controlled problem for the hydrogen heat exchanger. The system is fully specified by the temperature $T(z)$, the pressure $P(z)$ and the conversion $\xi(z)$. These variables are the three state variables of the system. Figure 3.1 illustrates the simplified hydrogen heat exchanger discussed in section 2.1.

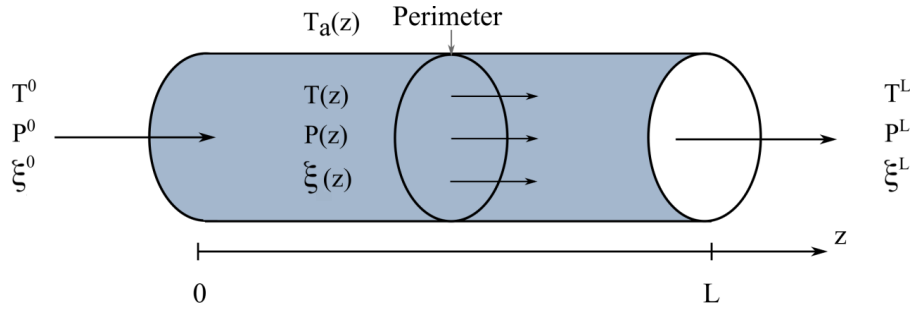

Figure 3.1: Simplified illustration of the heat exchanger.

The only variable that we control is the temperate of the utility, $T_a(z)$, which is our control variable. We now have

$$\begin{aligned} \mathbf{x}(z) &= \big[T(z), P(z), \xi(z)\big], \\ u(z) &= T_a(z). \end{aligned} \tag{3.6}$$

The constraints of the system are given by the balance equations

$$\begin{aligned} \frac{dT}{dz} &= f_T(\mathbf{x}(z), u(z)), \\ \frac{dP}{dz} &= f_P(\mathbf{x}(z)), \\ \frac{d\xi}{dz} &= f_\xi(\mathbf{x}(z)). \end{aligned} \tag{3.7}$$

We want to minimize the local entropy production (σ), discussed in Chapter 2.3, given by

$$\left(\frac{dS}{dt}\right)_{irr} = \int_0^L \sigma(\mathbf{x}(z), u(z))dz. \tag{3.8}$$

Now that we have recognized all the variables, the constraints and the function that we want to minimize, we can write the Hamiltonian of the heat exchanger

$$H(\mathbf{x}(z), u(z), \lambda(z)) = \sigma + \lambda_T(z) f_T + \lambda_p(z) f_p + \lambda_\xi(z) f_\xi. \tag{3.9}$$

Here the $\lambda(z)$'s are multiplier functions. In this case, the Hamiltonian is autonomous, meaning that it does not depend explicitly on z, and will therefore be constant through the heat exchanger.

By applying equation (3.4) to this Hamiltonian, we get the following $2(m+2)$ differential equations solving the optimally controlled problem

$$\begin{aligned}
\frac{dT}{dz} &= \frac{\partial H}{\partial \lambda_T} \\
\frac{dP}{dz} &= \frac{\partial H}{\partial \lambda_P} \\
\frac{d\xi}{dz} &= \frac{\partial H}{\partial \lambda_\xi} \\
\frac{d\lambda_T}{dz} &= -\frac{\partial H}{\partial T} \\
\frac{d\lambda_P}{dz} &= -\frac{\partial H}{\partial P} \\
\frac{d\lambda_\xi}{dz} &= -\frac{\partial H}{\partial \xi}.
\end{aligned} \tag{3.10}$$

There is only one control variable and equation (3.5) simplifies to

$$\frac{\partial H}{\partial T_a} = 0 \tag{3.11}$$

In order to complete the control problem, we have to consider the boundary conditions for the state variables.

The boundary condition for the conversions can be formulated in the following way

$$\begin{aligned} \xi^0 &= 0, \\ \xi^L &\quad \textit{specified}, \end{aligned} \tag{3.12}$$

which means, that at the inlet, the conversion are zero, and at the outlet, it is specified.

The four remaining boundary conditions are given by temperature and pressure at the in- and outlet T^0, p^0, T^L and p^L. In this problem, we want to handle both free and specified pressures and temperatures. Having free temperatures and pressures at the boundaries, corresponds to setting the respective multiplier functions to zero, as a free boundary is an unconstrained boundary. Thus, our last four boundary conditions are given by

$$\begin{aligned} T^0 &\quad \textit{specified} \quad \text{or} \quad \lambda_T^0 = 0 \\ T^L &\quad \textit{specified} \quad \text{or} \quad \lambda_T^L = 0 \\ P^0 &\quad \textit{specified} \quad \text{or} \quad \lambda_P^0 = 0 \\ P^L &\quad \textit{specified} \quad \text{or} \quad \lambda_P^L = 0. \end{aligned} \tag{3.13}$$

Calculation Details

The optimization was performed by using a routine first introduced by Johannessen [13]. This optimization routine has been used in several studies [26–29] and is composed of three parts.

Generation of Reference case: First a reference case is generated by using typical values from literature [12]. The reference case is used as a starting point for the optimization routine.

Numerical Optimization: By using input data from the reference case, a numerical optimization is performed by using a

coarse grid (6-30 points) with the Matlab 9.2-routine fmincon to create an initial guess for the optimal control problem.

Analytical Optimization: The optimal control problem as described in section 3.1.1 is solved by using the Matlab boundary value solver, bvp4c, with the result form the numerical optimization as initial guess.

The numerical optimization is performed before the analytical optimization to ensure that the optimization algorithm returns a global minimum.

Chapter 4

Cases

In this thesis, we will study two hydrogen liquefaction heat exchangers, operating at different conditions. Both follow the plate fin heat exchanger geometry as described in section 2.1. Figure 4.1 illustrates one chamber of the heat exchanger. The geometry of the heat exchanger is given in Table 4.1.

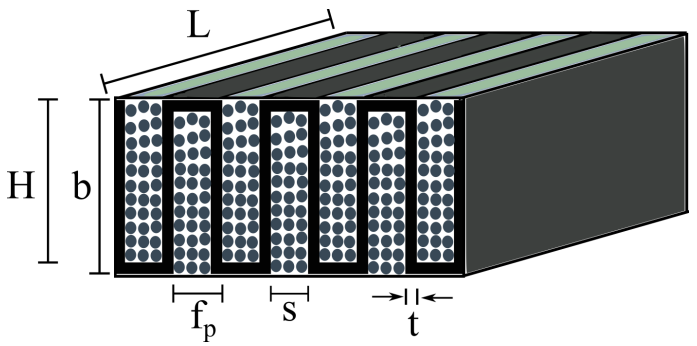

Figure 4.1: Illustration of one chamber filled with catalyst pellets in a plate fin heat exchanger.

In the first case, the inlet pressure is 19.6 bar. We will call this

Table 4.1: Geometry of plate fin heat exchanger.

Parameter	**Value**	**Unit**
Geometry of the total heat exchanger		
Length (L)	2	m
Hieght ($H_{heatexchanger}$)	1.5	m
Width (W)	0.8	m
Geometry of one chamber/layer of the heat exchanger		
Fin Hight (H)	$4 \cdot 10^{-3}$	m
Fin Thickness (t)	$3.5 \cdot 10^{-4}$	m
Fin Spacing (s)	$1.1 \cdot 10^{-3}$	m
Parting Sheet Distance (pt)	$1.5 \cdot 10^{-3}$	m

case the *20 bar case*. In the second case the inlet pressure is 80 bar. We will call this case the *80 bar case*.

In section 3.1, we saw that the optimization program is able to handle both free and specified temperatures and pressures at the boundary. In this study, we will fixate both the pressure and temperature at the inlet, as what happends upstream of the system is out of the scope of this study. Changing the temperature and pressure at the inlet will cause additional work in other parts of the hydrogen liquefaction prosess. We will aslo fix the temperature at the outlet, as it is necessary that the system reaches a specific temperature. The pressure at the outlet is free and will be optimized by the program.

We need to generate two reference cases (as described in section 3.1), one for each case. The reference cases are constructed by using a Matlab code made by Øivind Wilhelmsen [12] as a part of a study on different refrigerants in the hydrogen plate fin heat exchanger. We will use the same reference case as he used. In this reference case gaseous

hydrogen is used as refrigerant. The reference systems are obtained by solving the balance equations (see section 2.2) on the cold and hot sides of the plate fin heat exchanger (see figure 2.2).

In the Matlab code made by Wilhelmsen, the whole heat exchanger (described in section 2.1) is solved. In this heat exchanger, one sequence consists of four chambers/streams, two hot and two cold. The sequence is repeated 1034 times. The two cold streams are identical. The two hot streams are similar, in the sense that both contain catalyst pellets and hydrogen gas, but the chambers are operating at different conditions. As explained in section 2.1, we need to simplify this system in the optimization. The reference systems in this study are constructed by extracting the flow data from one of the hot streams together with the temperature profile of the cold stream.

At low temperatures, there will be constraints on what temperatures the utility may take. In our reference case, this is taken into account, as the cold stream is solved in the same way as the hot stream. In our optimization, this is not taken into account, and we do not put any restrictions on the temperature of the utility. This may result in profiles which may be difficult to realize in practice.

The optimized results will be compared to ideal gas calculations. There will also be a discussion on equipartition of entropy production and equipartition of forces. When finding the EoEP profiles, we "force" the local entropy prodcution to be constant. This is done by guessing a value for the local entropy production. Then the balance equations are solved for a constant local entropy production. This process is preformed until the boundary consitions are satisfied. The EoF solution is found the same way, only this time, the thermodynamic driving force ($\Delta 1/T$) is fixed. Calculation details on the equipartition theorems can be found in references [25, 28]. We will also have a look at the highways of our two heat exchangers. The highways are found by running several optimization with different temperature boundary conditions.

4.1 Case 1: 20 bar

The first case is the 20 bar case. As mentioned in Chapter 3, the optimization starts with a generation of a reference case. The reference case is used as a starting point in the optimization routine. All inlet and outlet conditions of the reference case are given in Table 4.2.

Table 4.2: In- and outlet condition in the reference heat exchanger, Case 1.

Parameter	**Value**	**Unit**
Inlet conditions		
Temperature	47.8	K
Pressure	$19.6{\cdot}10^5$	Pa
Mole fraction parahydrogen	0.7673	-
Mole fraction Orthohydrogen	0.2327	-
Molar flow rate	8.4433	mol/s
Outlet conditions		
Temperature	29.3014	K
Pressure	$19.361 \cdot 10^5$	Pa
Mole fraction parahydrogen	0.9363	-
Mole fraction Orthohydrogen	0.0637	-

In the reference case, hydrogen gas is used as refrigerant. Table 4.3 gives the flow data on the clod hydrogen stream. This data is only used in the generation of the reference case. In the optimization we consider the utility as a cooling medium with no restrictions on what temperatures it can take. In the reference heat exchanger a counter current flow is used. This means that the inlet of the cold stream is at the same position as the outlet of the hot stream.

In both cases, the molar flow rate of the system if fixed. We also assume a constant heat transfer coefficient. The heat transfer coefficient of the system is calculated by using data form the reference case. In the 20 bare case, the heat transfer coefficient is $U = 438.6578$.

Table 4.3: In- and outlet condition of the cold stream in the reference heat exchanger, Case 1.

Parameter	**Value**	**Unit**
Inlet conditions		
Temperature	28.9000	K
Pressure	$5.000 \cdot 10^5$	Pa
Molar flow rate	37.8766	mol/s
Outlet conditions		
Temperature	43.8366	K
Pressure	$4.9963 \cdot 10^5$	Pa

4.2 Case 2: 80 bar

Case 2, the 80 bar case, is similar to Case 1 in the sense that all the equations and all the geometry is unchanged. In Case 2, the inlet pressure of the hydrogen gas is increased to 80 bar. This changes some of the boundary condition. Table 4.4 gives all the boundary conditions for Case 2.

Increasing the pressure will influence many properties of the system, including the heat transfer coefficient. In the 80 bar case, the heat transfer coefficient is reduced compared to the 20 bar case. This is (among other things) due to a velocity dependence in the heat

transfer coefficient [47]. The new heat transfer coefficient is equal to $U = 279.1318$.

Table 4.4: In- and outlet condition in the reference heat exchanger, Case 2.

Parameter	**Value**	**Unit**
Inlet conditions		
Temperature	47.8	K
Pressure	$80{\cdot}10^5$	Pa
Mole fraction parahydrogen	0.7673	-
Mole fraction Orthohydrogen	0.2327	-
Molar flow rate	8.4433	mol/s
Outlet conditions		
Temperature	29.1444	K
Pressure	$79.884{\cdot}10^5$	Pa
Mole fraction parahydrogen	0.9470	-
Mole fraction Orthohydrogen	0.0530	-

Table 4.5 gives the flow data on the cold stream of the 80 bar case. As in Case 1, a counter current flow is used. This means that the inlet of the cold stream is at the same position as the outlet of the hot stream.

Table 4.5: In- and outlet condition of the cold stream in the reference heat exchanger, Case 2.

Parameter	**Value**	**Unit**
Inlet conditions		
Temperature	28.3900	K
Pressure	$4.6300 \cdot 10^5$	Pa
Molar flow rate	26.2811	mol/s
Outlet conditions		
Temperature	46.3743	K
Pressure	$4.6282 \cdot 10^5$	Pa

Chapter 5

Results and Discussion

5.1 Consistency of the System

A greater part of this study concerned implementing the multiparameter equation of state discussed in section 2.4 and integrating the equation into the optimization framework discussed in Chapter 3.1. We will therefore discuss the consistency of the system to justify that the final optimized results are valid. In this section, there will also be a summary of important thermodynamic properties of the hydrogen gas and a comparison of the real and ideal gas behavior, which will be used in the further discussion of the optimized systems.

To study the consitency of the system we will use a database developed by the *National Institute of Standards and Technology* (NIST), called *REFPROP*. This database provides the most accurate thermophysical models for pure fluids and mixtures over a wide range of fluid conditions including liquid, gas, and supercritical phases. It contains critically evaluated mathematical models, with the goal of representing the properties to within the uncertainty threshold of the underlying experimental data used in the development [34].

5.1.1 Consistency of Equations

Case 1

Figures 5.1 - 5.3, show the density, heat capacity and enthalpy as a function of temperature, at a pressure of 20 bar. For simplicity, a constant pressure is used.

Calculation details on the equation of state are given in Appendix A.1 and A.3. All equations used in this study have been compared to the REFPROP database. The comparison gives a relative error within the the order of magnitude 10^{-8}.

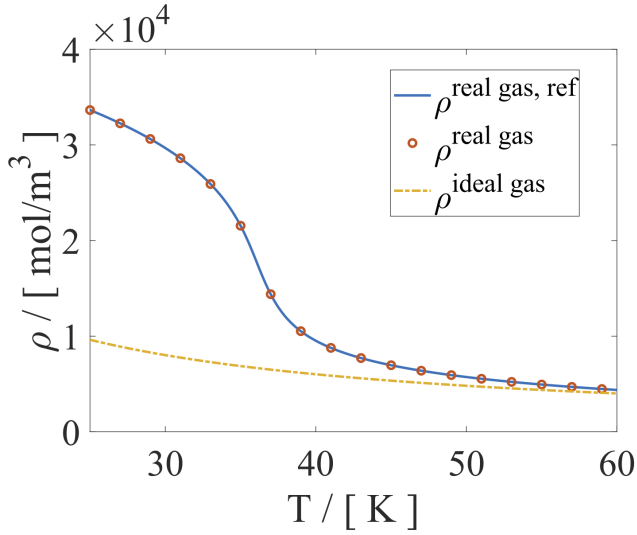

Figure 5.1: Density of parahydrogen as a function of temperature at 20 bar. The solid line is obtained by using the REFPROP database, the circles are calculated by using the equation of state introduced in section 2.4, and dot-dashed line represent ideal gas calculations.

Figure 5.1 shows the density of parahydrogen as a function of temperature. We observe that the real gas density of parahydrogen in-

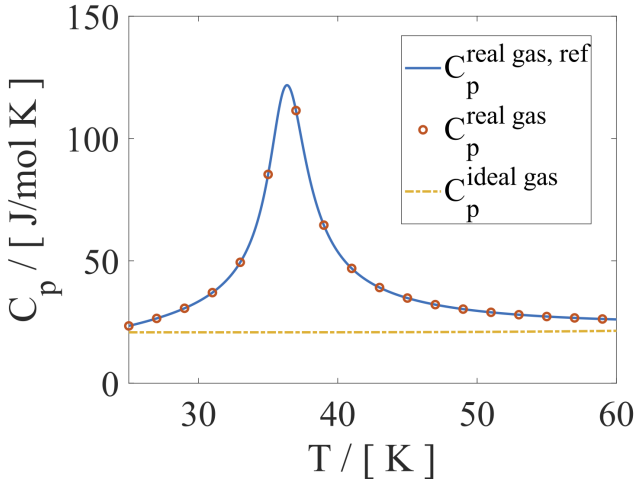

Figure 5.2: Parahydrogen heat capacity as a function of temperature at 20 bar. The solid line is obtained by using the REFPROP database, the circles are calculated by using the equation of state introduced in section 2.4, and dot-dashed line represent ideal gas calculations.

creases suddenly at low temperatures. This behavior is quite different from the ideal gas behavior. At 25K, the real gas density is more than three times greater than the ideal gas density. Because the density is one of the fundamental variables in the equation of state used in this study, the behavior of the density will have a great impact in the entire system. One example is the gas velocity, which will decreases as the density increases.

Figure 5.2 demonstrates the same non-ideal behavior. The figure shows the heat capacity of parahydrogen as a function of temperature. The first most obvious observation we make is the peak at about 36K. We also observe that the real gas heat capacity is higher than the ideal gas heat capacity in the entire interval. Thus, the real gas system will

demand more energy when cooled down. As there is a peak in the heat capacity, there will be a region in the heat exchanger where the system will demand even more energy. The two figures show the same tendency: at low temperatures, the hydrogen gas does not behave as an ideal gas. We will therefore expect the optimized temperature profiles of the real gas system and ideal gas system to behave quite differently.

The behavior of the density and heat capacity of orthohydrogen is similar to the behavior of parahydrogen and is therefore left out.

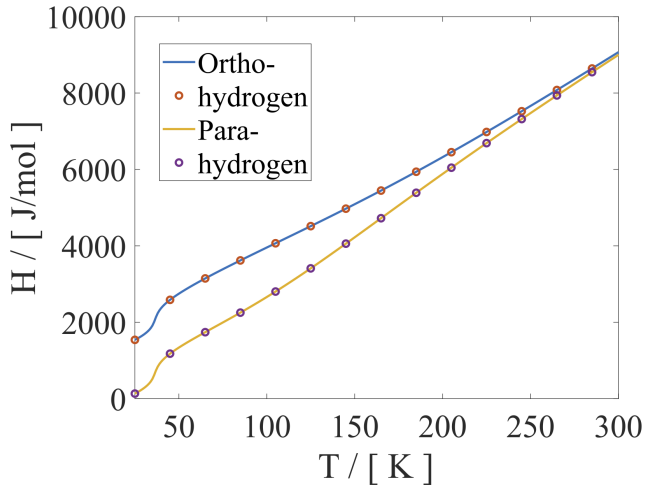

Figure 5.3: Enthalpy of parahydrogen and orthohydrogen as a function of temperature at 20 bar. The solid lines are obtained by using the REFPROP database and the circles are calculated by using the equation of state introduced in section 2.4.

In Figure 5.3, the enthalpy of both parahydrogen and orthohydrogen is plotted as a function of temperature. In this plot, the temperature range is extended to illustrate the different behavior of the

hydrogen gas at cryogenic and ambient temperatures.

At low temperatures, the enthalpy of orthohydrogen is higher than the enthalpy of parahydrogen. As mentioned in the introduction (section 1.2), the eigen energy of orthohydrogen is higher than the eigen energy of parahydrogen. This is due to the different spin configurations of the hydrogen isomers. At low temperatures, the thermal energy of the system will decrease. As orthohydrogen requires more energy than parahydrogen, at low temperatures, the orthohydrogen state will be less likely, and the system will "fall into" the parahydrogen state. This is what causes the gap between the enthalpies in Figure 5.3. In order to achieve consistency and the correct gap in the enthalpy and entropy, we had to alter the reference values for the enthalpy and entropy in comparison to what is given by REFPROP.

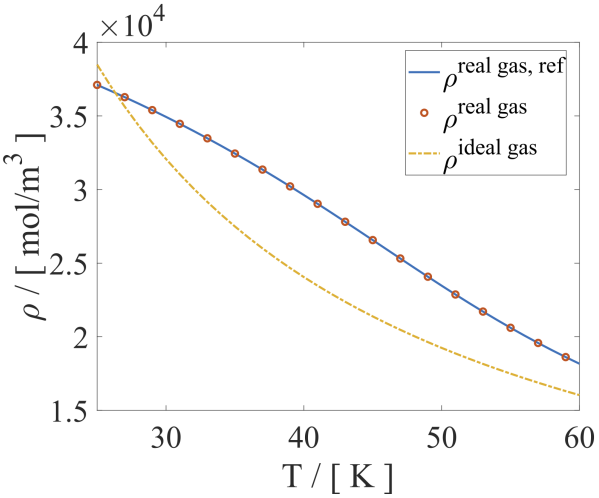

Figure 5.4: Density of parahydrogen as a function of temperature at 80 bar. The solid line is obtained by using the REFPROP database, the circles are calculated by using the equation of state introduced in section 2.4, and dot-dashed line represent ideal gas calculations.

Case 2

Figures 5.4 - 5.6, show the density, heat capacity and enthalpy as a function of temperature, at a pressure of 80 bar. For simplicity, a constant pressure is used.

The density of parahydrogen at 80 bar is plotted as in Figure 5.4. There are several things worth noticing in this figure. First, we notice that the density does not have the same jump as we saw in Case 1. Secondly, we note that the average density in this case is higher than in Case 1. This third thing we notice is that the real gas and ideal gas density is not dramatically different.

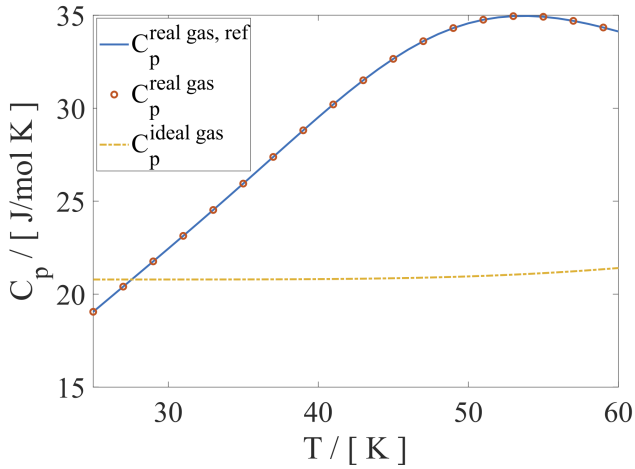

Figure 5.5: Heat capacity of parahydrogen as a function of temperature at 80 bar.The solid line is obtained by using the REFPROP database, the circles are calculated by using the equation of state introduced in section 2.4, and dot-dashed line represent ideal gas calculations.

Figure 5.5 shows the heat capacity of parahydrogen at 80 bar. We

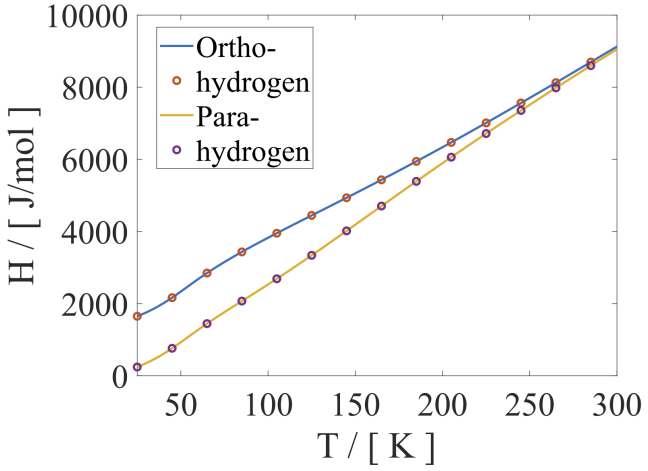

Figure 5.6: Enthalpy of parahydrogen and orthohydrogen as a function of temperature at 80 bar. The solid lines are obtained by using the REFPROP database and the circles are calculated by using the equation of state introduced in section 2.4.

observe that there is no longer a peak in the heat capacity. We also note that the overall heat capacity of Case 2 is lower than in Case 1.

The enthalpy of both ortho- and parahydrogen is plotted in Figure 5.6. We observe that the enthalpy gap between ortho- and parahydrogen still is significant in the 80 bar case. When the temperature decrease, the gap increase.

To summarize, in Case 1, the difference between the ideal gas and real gas in terms of density and heat capacity is significant. We also observed some sudden changes in the properties of hydrogen gas at low temperatures. In Case 2, we observe that the real gas behavior of the system did not have any sudden changes at low temperatures. We have also seen that the equations presented in section 2.4 is in agreement with the data given in by the REFPROP database. The

properties discussed in this section will be important in the discussion of the optimizations.

Gibbs Energies

Gibbs free energy and Gibbs energy of the reaction are two convenient properties when checking for consistency in a system. When plotted as a function of chemical composition at constant temperature and pressure, the two functions have either a minimum (Gibbs free energy) or a zero (Gibbs energy of the reaction) when the system is in chemical equilibrium [32, 33, 37].

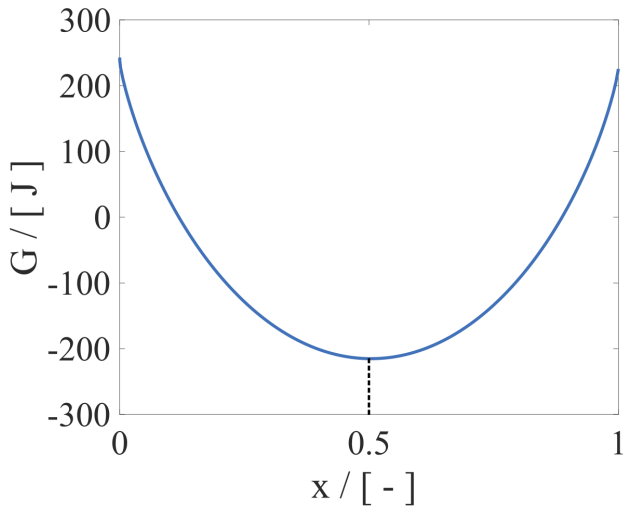

Figure 5.7: Gibbs free energy of the mixture as a function of parahydroge mole fraction at 77.3K.

By using the equation for the equilibrium mole fraction (see Appendix A.4), we found that at $T = 77.3$K, the equilibrium composition of parahydrogen is 50%. Figure 5.7 shows the Gibbs free energy at

77.3K, plotted as a function of chemical composition of parahydrogen. We observe that the Gibbs free energy has a minimum corresponding to a mole fraction of $x = 0.5$.

The Gibbs energy of the reaction is zero when the system is in chemical equilibrium [32,33,37]. Figure 5.8 shows the Gibbs energy of the reaction as a function of chemical composition of parahydrogen at 77.3K. From Figure 5.8 we can read an equilibrium composition 50% parahydrogen at 77.3K which is consistent with what discussed above.

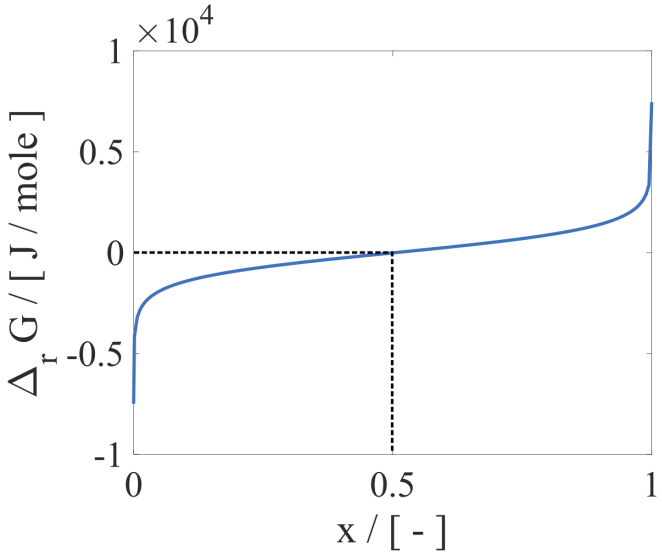

Figure 5.8: Gibbs energy of the reaction as a function of parahydrogen mole fraction at 77.3K

The equilibrium mole fraction of parahydrogen as a function of temperature is given in Figure 5.9. The temperature range is set from 25K to 80K, which covers the range that we want to study in the optimization. The figure shows calculations of the equilibrium mole fraction (blue line), given in literature [12], see also Appendix A.4.

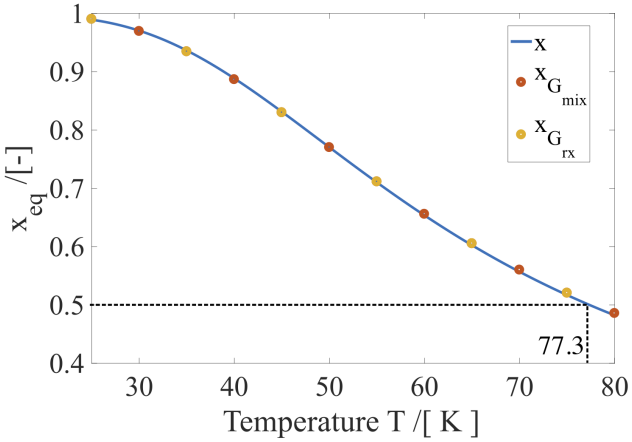

Figure 5.9: Equalibrium mole fraction as a function of temperature. The blue solid line is the equilibrium mole fraction given in literature (see AppendixA.4), the yellow dots are obtained by using Gibbs energy of the reaction, and the red dots are obtaind by using Gibbs energy of the mixture.

The yellow dots represent the equilibrium mole fraction of parahydrogen obtained by using the Gibbs free energy of the mixture, and the red dots are the equilibrium mole fractions found by using the Gibbs energy of the reaction. Figure 5.9 shows good agreement between expression given in literature and the equations implemented in this study, which gives us a further confirmation that the system is consistent.

5.1.2 Consistency in the Optimization

Checking for consistency in the equations is not sufficient to validate the optimization results. It is also necessary to check for consistency in the optimization.

As described in section 2.3, we have two options when calculating the entropy production in a system. We can either use the local entropy balance or the total entropy balance over the system. The two formulations are equivalent, as shown in section 2.3. In this study, both of them are used. The local entropy balance formulation is used in the optimization, and the total entropy balance is used as a consistency check.

We also need to check the energy balance of the system. The energy balance is defined as the energy flowing out of the system minus the energy lowing in to the system. As we saw in the derivation of the entropy production, there will be energy flowing through the in- and outlet of the heat exchanger, as well as though the walls.

Table 5.1: Relative error of the entropy production check, and the difference between the energy going in and out of the optimized heat exchanger, Case 1.

	Value	**Unit**
Entropy Production Check (relative error)	$6.8713 \cdot 10^{-06}$	-
Energy Balance (difference)	0.0036	J/s

Table 5.1 gives the relative error of the entropy production check, described above, and the difference in energy flowing in and out of the heat exchanger. In this table, Case 1 is used as an example. In all optimizations preformed in this study, the entropy production check and the energy balance check has been performed. The energy balance are check to be in the same order of magnitude (or smaller) as presented in Table 5.1 and the relative error of the entropy production checks are all within the accuracy of the optimization, which has a tolerance on 10^{-5}.

We also need to check the properties of the optimal control problem discussed in Chapter 3.1. As our Hamilton function is autonomous, the

Hamiltonian should be constant. Figure 5.10 shows the Hamiltonian for the 20 bar optimized case (which will be discussed in details in section 5.2.2).

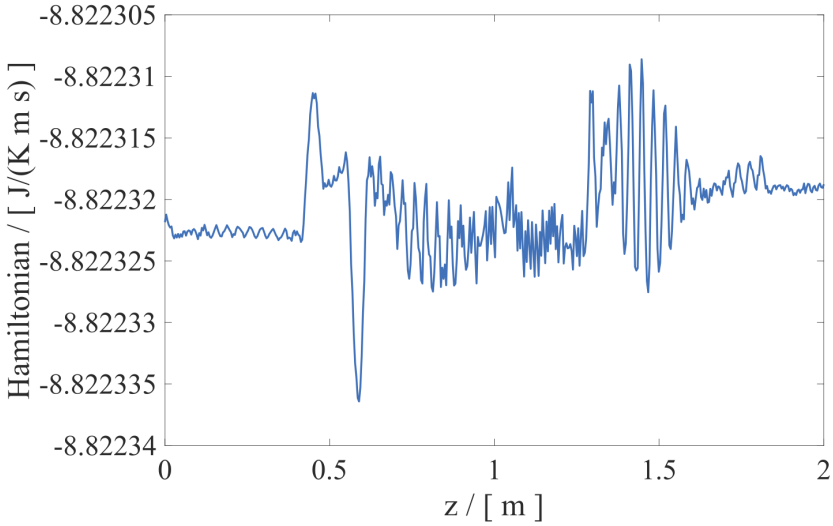

Figure 5.10: The Hamiltonian of Case 1.

The relative deviation of the Hamiltonian is in the order of magnitude 10^{-6}, which means that the fluctuations observed in Figure 5.10 are caused by the accuracy of the optimization, and the Hamiltonian can be considered constant.

We also need to check the optimization relation in equation (3.11)($\frac{\partial H}{\partial T_a} = 0$ for the optimized case). Figure 5.11 shows the derivative of the optimal Hamiltonian (H) with respect to the optimal temperature of the utility (T_a).

As we can see, the relation from equation 3.11 is fulfilled at every point in the heat exchanger to within the accuracy of the optimization.

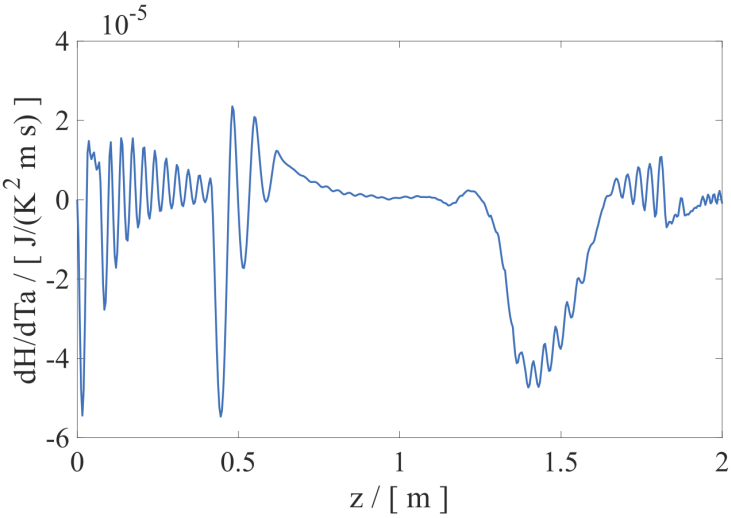

Figure 5.11: The derivative of the Hamiltonian with respect to the temperature of the utility, Case 1.

All checks presented in this section are also performed on the 80 bar case. All checks preformed on the 80 bar case give results within the accuracy of the optimization. This confirms that the equations are implemented correctly, and that the formulation of the optimal controlled problem is correct.

5.2 Case 1

5.2.1 The Reference Case

The first case we are going to discuss is the 20 bar case described in section 4.1. Before presenting the optimal path, we want to look at the reference case profiles. As described in section 4, the reference case is using hydrogen as cooling medium.

The temperature profiles of the reference heat exchanger is plotted in Figure 5.12. The blue dashed line represents the cold streams of the plate fin heat exchanger. We call this the temperature of the utility (T_a). The red solid line is the temperature of the hydrogen gas inside the heat exchanger (T).

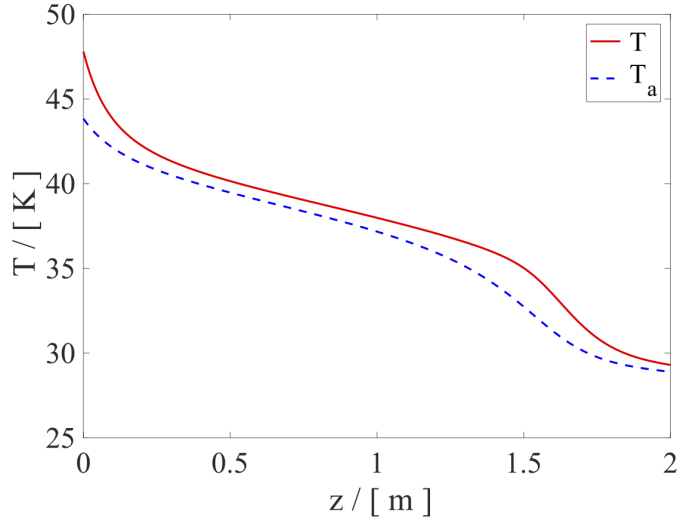

Figure 5.12: Temperature (T) inside the heat exchanger (red line) and the temperature of the utility (T_a) (dashed blue line) as a function of position. Reference Case 1.

In Figure 5.13 the local entropy production (LEP) of the reference heat exchanger is plotted as a function of position. As discussed in section 2.3, there are three contributions to the entropy production in this system, namely the heat transfer through the walls (σ_q), the spin-isomer reaction (σ_{rx}) and the pressure drop in the heat exchanger(σ_p). All three contributions are plotted in Figure 5.13 together with the total local entropy production (σ_{total}), which is the sum of the three

contributions.

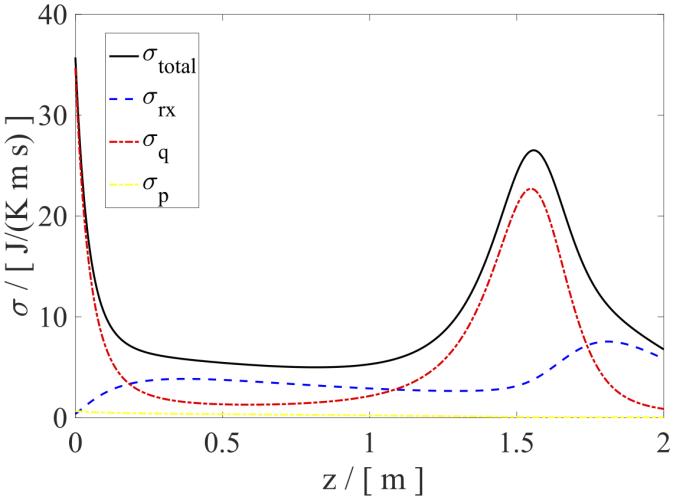

Figure 5.13: Local entropy production (LEP) as a function position in the reference heat exchanger. The yellow dot-dashed line represents the LEP associated with frictional flow, the red dot-dashed line represents the heat transfer contribution to the LEP and the blue dashed line represents the contribution form the hydrogen spin-isomer conversion reaction to the LEP. The black solid line is the sum of the three contributions.

The LEP profiles show that σ_q is the main source of entropy production in the system. This is further confirmed by Table 5.2. Almost 60% of the overall entropy production in the system is caused by the heat transfer. From equation (2.24) and Table 2.1, we know that $\Delta(1/T) = 1/T - 1/T_a$ is the driving force of the σ_q term. Looking at Figure 5.13, we observe that there are two peaks in the local entropy production (one at the inlet and one around z = 1.5) . These two peaks coincide with positions in the heat exchanger where the temper-

Table 5.2: Total entropy production (TEP) in the 20 bar reference heat exchanger.

TEP	**Value**	**Unit**
Total	20.2799	J/Ks
Heat	12.1112	J/Ks
Reaction	7.6799	J/Ks
Pressure drop	0.4888	J/Ks

ature difference (ΔT) (see Figure 5.12) deviates the most. Comparing Figure 5.12 with Figure 5.13 we notice that ΔT is an important factor in the system, and changes in ΔT will influence the overall entropy production.

The blue dashed line in Figure 5.13 is the local entropy production associated with the reaction (σ_{rx}). About 38% of the overall entropy production in the heat exchanger originates from this term. Figure 5.14 shows the equilibrium mole fraction of parahydrogen (dot-dashed blue line) and the mole fraction of parahydrogen (solid black line). We observe that the system is never in (chemical) equilibrium. The entropy production associated with the spin-siomer conversion reaction depends on the Gibbs energy of the reaction ($\Delta_r G$). As already discussed, the Gibbs energy of the reaction is zero when the system is in chemical equilibrium. A system far away from chemical equilibrium will therefore produce more entropy and will be less energy efficient.

Figure 5.13 also shows that the pressure-drop related entropy production has a minor effect on the overall entropy production, as only about 2% of the overall entropy production originates from this term. The pressure in this heat exchanger decreases with only about 1%.

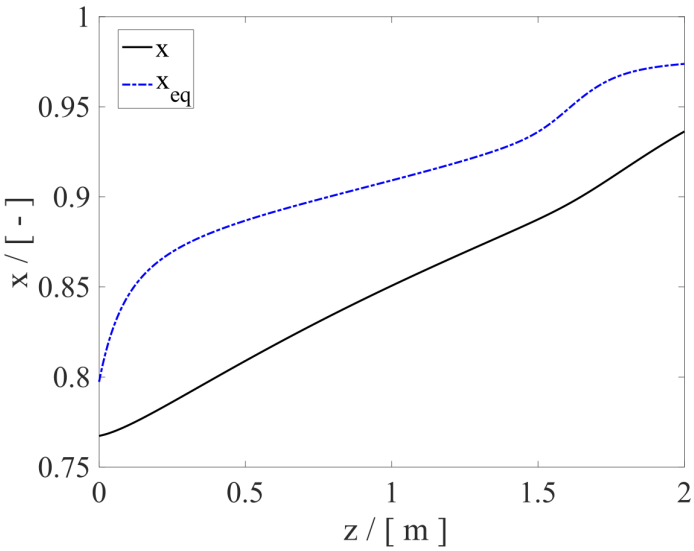

Figure 5.14: Equilibrium mole fraction of parahydrogen as a function position in the heat exchanger. The blue dot-dashed line is the equilibrium mole fraction, and the black solid line is the mole fraction inside the reference heat exchanger, Case 1.

5.2.2 The Optimal Path

An optimization, as described in Chapter 3 was performed on the reference heat exchanger described in section 5.2.1. In this optimal controlled problem, all boundary conditions were fixed, except the pressure at the outlet as described in Chapter 4. The optimized pressure is slightly increased from $19.361 \cdot 10^5$Pa to $19.376 \cdot 10^5$Pa.

Figure 5.15 shows the optimized temperature profiles of the heat exchanger as a function of position. We observe that the optimization results give a temperature profile where the difference between the temperature of the utility and the hydrogen gas (ΔT) is more con-

stant. We also observe that there is a small "plateau" in the temperature profile in the middle of the heat exchanger. This small plateau coincides with the peak in the heat capacity in Figure 5.2. As mentioned in section 5.1.1, when the heat capacity is higher, the system will cool down slower. This is what we observe as the plateau in Figure 5.15.

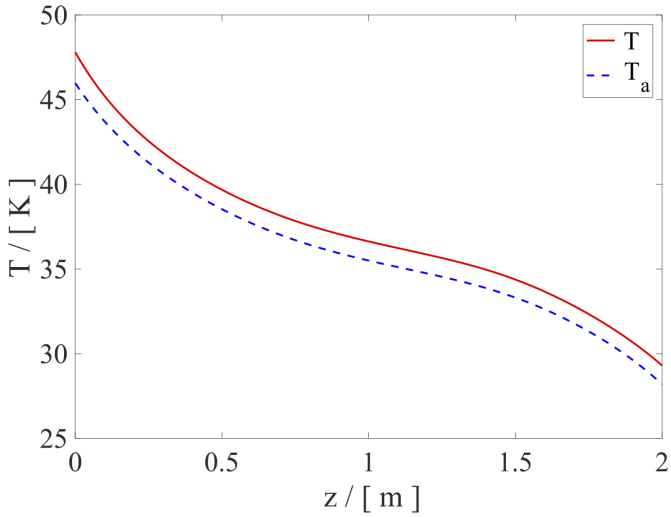

Figure 5.15: Optimized temperature profiles, Case 1. The red solid line is the temperature (T) inside the heat exchanger and the dashed blue line is the temperature of the utility (T_a).

Figure 5.16 shows the optimized local entropy production profiles and Table 5.3 gives the total entropy production of the system. The entropy production in the optimized heat exchanger is reduced by 14.90%. Most of the reduction is due to a reduction in the heat transfer term, which is reduced by 23.46%.

In both the reference and the optimal case, the heat transfer is the main entropy production source. At very low temperatures, the

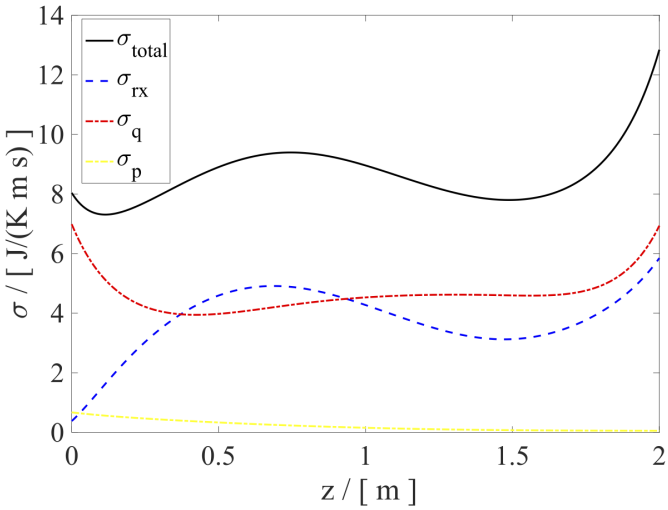

Figure 5.16: Optimized local entropy production profiles, Case 1. The yellow dot-dashed line represents the LEP associated with frictional flow, the red dot-dashed line represents the heat transfer contribution to the LEP and the blue dashed line represents the contribution form the hydrogen spin-isomer conversion reaction to the LEP. The black solid line is the sum of the three contributions.

Table 5.3: Total entropy production (TEP) in the optimized heat exchanger, Case 1.

TEP	**Value**	**Unit**
Total	17.2582	J/Ks
Heat	9.2701	J/Ks
Reaction	7.5476	J/Ks
Pressure drop	0.4405	J/Ks

heat transfer will be a significant source of entropy production as the driving force for this LEP term is $\Delta 1/T$. If ΔT is fixed and we decrease the temperature, this term will increase.

Comparing the local entropy production profiles of the reference case and optimized case, we observe some differences. The most significant difference between the two profiles is the smoothing of the LEP curves.

In the optimized case, the temperature profiles of the utility and the hydrogen gas are relatively parallel (compared to the reference case). This results in more constant local entropy production profiles. Comparing the local entropy production profiles in the reference case and optimal case, we observe that there are regions in the reference heat exchanger where the local entropy production is considerably lower than in the optimal case. However, as the optimal case does not have any peaks, the overall total entropy production is reduced. It seems like the optimal heat exchanger is characterized by a relative constant entropy production (compared to the reference case).

We also note that total entropy production due to the spin-isomer reaction σ_{rx} is reduced by 1.72%. The mole fraction and equilibrium mole fraction of parahydrogen is plotted in Figure 5.17.

We observe that the optimized system is not closer to equilibrium than the reference system. The hydrogen spin-isomer reaction taking place in the heat exchanger is a slow reaction [12]. As a result of the slow reaction, the system does not have time (or freedom) to equilibrate. This is why there are so little change in σ_{rx}.

Earlier studies have observed that optimized reactors/heat exchangers can be split into two parts [28]. In the first part of the reactor/heat exchanger, the system will be in the *reaction mode*, as the reaction is dominating the system, and is the main source of entropy production. In the other part of the reactor/heat exchanger, the system is in the *heat transfer mode*. In this section, the heat transfer is dominating the system, and is the main source of entropy production. These opti-

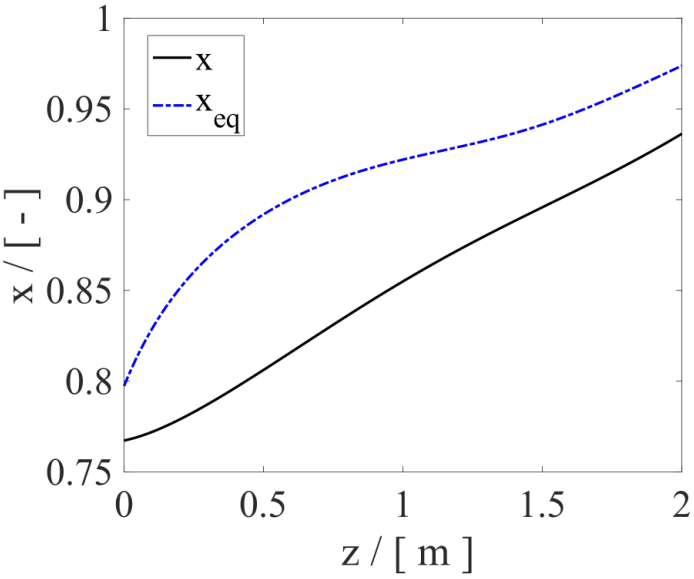

Figure 5.17: Optimized mole fraction and equilibrium mole fraction of parahydrogen, Case 1. The blue dot-dashed line represents the equilibrium mole fraction, and the black solid line represents the mole fraction inside the heat exchanger.

mized reactors/ heat exchangers prefer to finish some of the reaction in the beginning of the reactor, which resultes in systems closer to equilibrium than our hydrogen liquefaction system.

As we can see in Figure 5.16 and 5.17, this is not the case in our heat exchanger. As mentioned, the hydrogen spin-isomer reaction is a rather slow reaction compared to for example chemical reactions studied in reference [28]. We therefore have an optimized system, where the reaction and heat transfer are almost equally important sources of entropy production through the system. We will come back to what this implies for the system.

5.2.3 The Role of a Real Gas Equation of State

The real gas equation of state discussed in section 2.4 is a rather complicated and expensive equation of state when it comes to computation time. It is therefore interesting to compare the results to the much simpler ideal gas equation of state, to see how much is gained by applying the more complicated equation.

Figure 5.18 shows the temperature profiles of the ideal gas optimized system. Comparing the temperature profile to the real gas temperature profile in Figure 5.15, we observe that the ideal gas formulation of the problem allows a much smaller ΔT than the real gas formulation. In the real gas case, the average temperature difference is $\Delta T_{average} = 1.1547$, in the ideal gas case, we have $\Delta T_{average} = 0.5703$.

As we saw in Figure 5.2, the ideal gas heat capacity of hydrogen is much lower than the real gas heat capacity. When the heat capacity is lower, the system will cool down easier, which results in a tighter match between the temperature profiles. We also observe that the ideal gas temperature profile does not have the plateau. This originates also from the heat capacity, as the ideal gas heat capacity does not have a peak (see Figure 5.2).

Table 5.4: Total entropy production (TEP) in the optimized ideal gas heat exchanger, Case 1.

TEP	**Value**	**Unit**
Total	11.6251	J/Ks
Heat	2.3208	J/Ks
Reaction	7.5681	J/Ks
Pressure drop	1.7362	J/Ks

Figure 5.19 shows the local entropy production profiles of the optimized system, using ideal gas law as equation of state. Table 5.4 gives

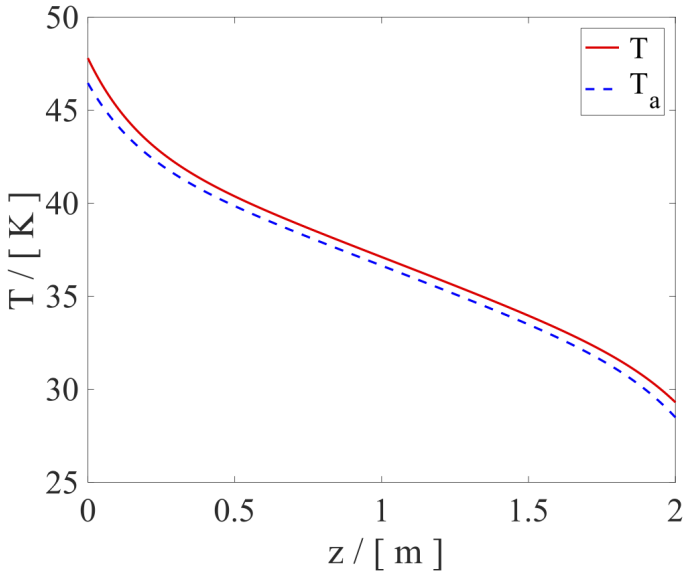

Figure 5.18: Optimized ideal gas temperature profiles, Case 1. The red solid line is the temperature (T) inside the heat exchanger and the dashed blue line is the temperature of the utility (T_a).

the total entropy production. The figure illustrates the effects of the small ΔT, as σ_q is reduced by an order of magnitude compared to the reference case.

One rather important property of the ideal gas case concerns the frictional flow term σ_p, which is almost four times larger than the real gas case. As discussed in section 5.1.1, the ideal gas density is lower than the real gas density. When the density decrease, the velocity of the system increases, as the total flow rate of the system is fixed. We saw in Table 2.1 that the velocity is the driving force of the frictional flow, which explains why this LEP term is increased in the ideal gas case.

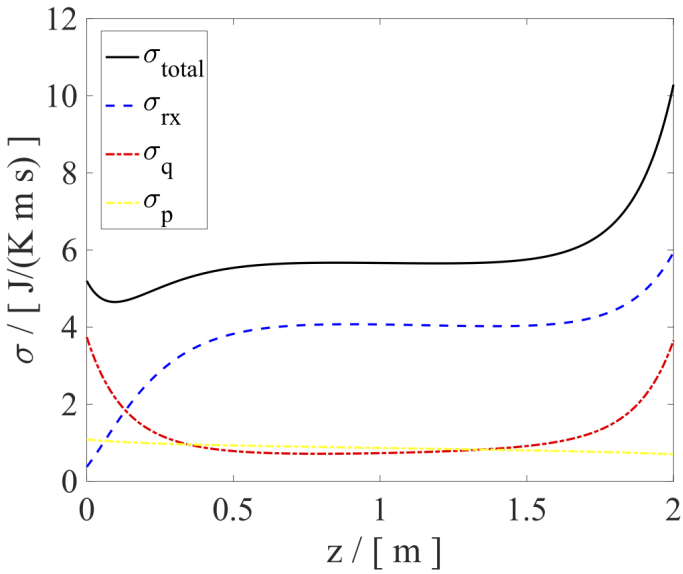

Figure 5.19: Optimized ideal gas local entropy production profiles, Case 1. The yellow dot-dashed line represents the LEP associated with frictional flow, the red dot-dashed line represents the heat transfer contribution to the LEP and the blue dashed line represents the contribution form the hydrogen spin-isomer conversion reaction to the LEP. The black solid line is the sum of the three contributions.

Figures 5.18 - 5.19 and Table 5.4 illustrate that ideal gas would not be a good approximation in this case. We saw in section 5.1.1 that the real gas behavior of hydrogen at low temperatures is quite different than the ideal gas behavior. It is therefore not a surprise that using the ideal gas equation of state in the optimization routine, results in an unrealistically small ΔT. If one applies the ideal gas equation of state, one will end up with a system which is in fact quite far away from the state of minimum entropy production.

5.2.4 Equipartition Theorems and Highway in State Space

The equipartition theorems describes optimal reactor/ heat exchanger design for a system with a sufficient amount of control variables. As discussed, this is not the case in our heat exchanger, as there is only one control variable and three state variables. However, Johannessen et al. [28] proposed a hypothesis concerning systems with too few control variables. This hypothesis states that EoEP and EoF are good approximations for systems that have sufficient *freedom*.

Figure 5.20 shows the temperature profiles of the heat exchanger. The black solid line is the optimal temperature profile, the blue dashed line is the EoEP temperature and the green dot-dashed line is the EoF temperature.

Figure 5.21 shows the local entropy production profiles of the optimization, EoEP and EoF. Table 5.5 gives the total entropy production in the reference case, the optimal case, EoEP and EoF. The Table also gives the improvement or percentage decline in the total entropy production compared to the reference case.

Table 5.5: Total entropy production of the reference case, optimal case, EoEP and EoF and improvement compared to the reference case, Case 1.

TEP	Value	Unit	Improvements
$\text{TEP}_{Reference}$	20.2799	J/Ks	-
$\text{TEP}_{Optimal}$	17.2582	J/Ks	14.90 %
TEP_{EoEP}	17.6705	J/Ks	12.87 %
TEP_{EoF}	18.1623	J/Ks	10.44 %

The optimal path of the system is not characterized by constant

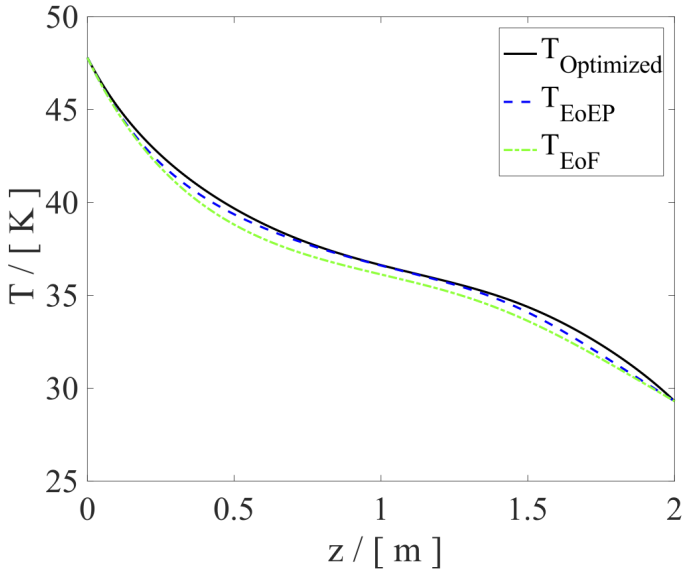

Figure 5.20: Temperature profile of the optimized case (black solid line), the EoEP temperature profile(blue dashed line) and the EoF temperature profile (green dot-dashed line) as a function of position, Case 1.

entropy production or constant driving forces (not shown). As mentioned, the system that we are studying here does not fulfill all the assumptions made in the equipartition theorems, which means that we would not expect the optimal system to have constant local entropy production or constant driving forces in the entire heat exchanger. According to Johannessen, we would expect equipartition of entropy production and equipartition of forces approximates the optimal solution.

We observe that the EoEP temperature profiles follows the optimal profiles rather well and that the total entropy production of the EoEP

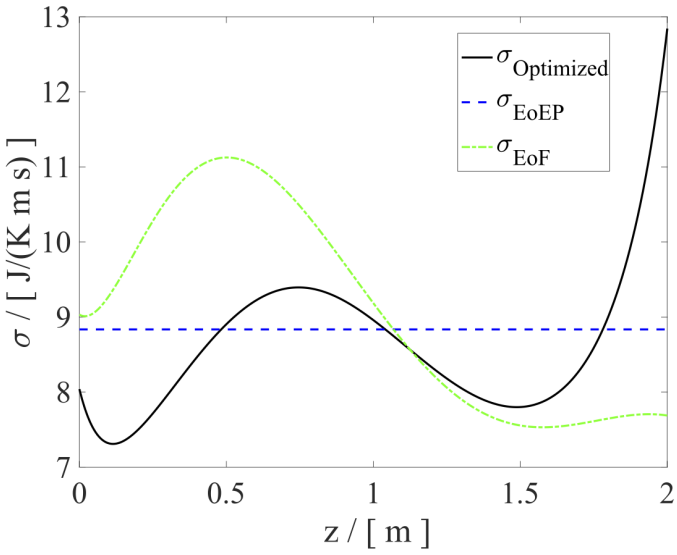

Figure 5.21: Local entropy production (LEP) of the optimized case (black solid line), the EoEP LEP profile (blue dashed line) and the EoF LEP profile (green dot-dashed line) as a function of position, Case 1.

solution differs from the optimal solution by only 2.39%.

In 2004, Johannessen et al. [29] studied a SO_2 reactor. During this study, the hypothesis cited in section 2.3 was developed. Johannessen and coworkers observed that sections in the optimal reactor, had constant entropy production and constant thermodynamic driving forces.

The SO_2 reactor that Johannessen studied was characterized by the reaction and heat transfer modes. The parts of the SO_2 reactor with constant local entropy production was characterized by the heat transfer mode. In the SO_2 reactor, most of the chemical reaction took place in the first part of the reactor (when the system is in reaction mode). When the system entered the heat transfer mode, the effects

of the chemical reaction and pressure drop was very small compared to the heat transfer. This resulted in only one effective state variable and one control variable and the first assumption of equipartition theorems (see section 2.3.2) is (approximately) satisfied. As a result of this, the system had enough freedom for EoEP and EoF to apply in this section of the reactor.

Our heat exchanger is not characterized in the same way, as we do not observe the heat transfer and reaction modes. We would therefore not expect the optimal system to have sections with constant entropy production, as the first assumption in the equipartition theorems is not satisfied in our hydrogen liquefier, and the system in general does not have enough freedom to satisfy EoEP and EoF. We therefore do not observe a constant local entropy production or constant thermodynamic driving forces (not shown) at any point in the heat exchanger.

The ortho- para conversion reaction is a rather slow reaction compared to chemical reactions in earlier studies. Also, the equilibrium composition of parahydrogen depends strongly on the temperature (see figure 5.9). This slow and temperature dependent nature of our spin-isomer reaction results in a system which is further away from equilibrium than systems studied before and it is what causes the system to enter neither the reaction mode nor the heat transfer mode.

Even though the system is not characterized by sections with constant entropy production, the hypothesis proposed by Johannessen still applies, as EoEP (and to some degree also EoF) may be good strategies for energy efficient operation of the hydrogen liquefier.

It is also worth mentioning that there may be practical difficulties concerning achieving the optimal path in a real heat exchanger, and in industrial application, the deviations between the achievable path and the optimal path may be of more importance. When comparing the optimal and the reference case, we have seen that hydrogen gas is not the best choice of refrigerant in this particular case. Achieving the optimal temperature profile of the utility may be done by using mixed

refrigerants. There have been several studies on using a mixture of neon and helium as refrigerant [12, 15]. It may be possible to find a neon to helium ratio which results in a temperature profile of the utility which is close to the optimal. However, this needs to be investigated further.

Figure 5.22 shows six out of 30 optimized temperature profiles with different inlet temperature boundary conditions.

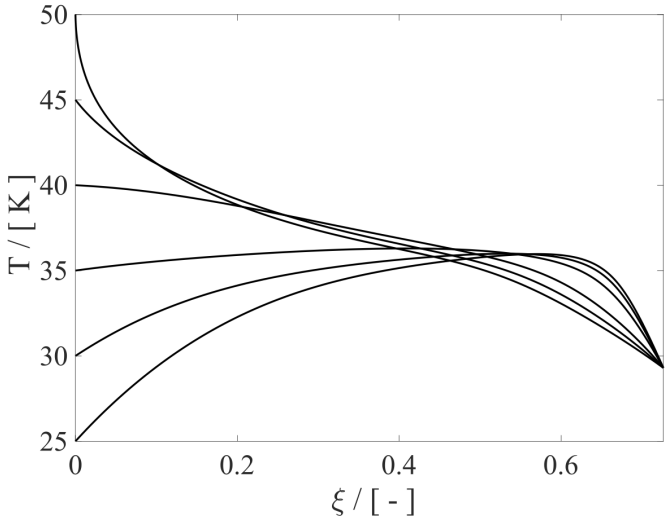

Figure 5.22: Optimized temperature profiles for different inlet temperatures as a function of the degree of the reaction. The inlet temperatures plotted in the figure is: $T^0 = 50$K, $T^0 = 45$K, $T^0 = 40$K, $T^0 = 35$K, $T^0 = 30$K, $T^0 = 25$K, Case 1.

As described in section 2.3, the highway in state space is a property that has been observed for a wide range of chemical reactor systems.

For a system with a highway, optimal solutions with different boundary conditions, will, after some equilibration and adjustments, follow a very similar "temperature path" when plotted as a function of the degree of reaction [28]. This common path is called the highway in state space and is characterized by constant local entropy production.

We do not observe a highway in Figure 5.22, as the different solution do not follow the same path. As discussed, in our heat exchanger the reaction and the heat transfer are (almost) equal contributors to the entropy production through the entire system. As a result of this, the first assumption in the theorems of EoEP and EoF is not satisfied and we do not have sections of constant local entropy production and thermodynamic forces. As the highway is characterized by the heat transfer mode (and constant local entropy production) Figure 5.22 is in consistency with the results above.

5.3 Case 2

5.3.1 The Reference Case

The second case we are going to study is the 80 bar case described in section 4.2. Before discussing the optimal path, we will have a closer look at the reference case.

Figure 5.23 shows the reference temperature profiles of the system.

Figure 5.24 show the local entropy production of the 80 bar reference case, and Table 5.6 gives the total entropy production. The local entropy production profiles of reference Case 2 are rather different from the profiles of reference Case 1. The main difference is the heat transfer term, which is significantly lower in this reference case. As we observe in figure 5.23, this is not due to a reduction in ΔT, but due to a reduction in the heat transfer coefficient. Decreasing the heat transfer coefficient, will reduce the heat flux J_q (see equation (2.19)),

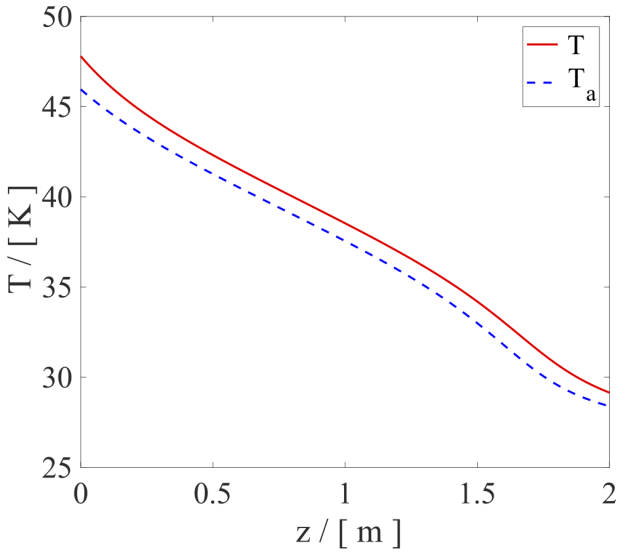

Figure 5.23: Temperature (T) inside the reference heat exchanger (red line) and the temperature of the utility (T_a) (dashed blue line) as a function position, Case 2.

Table 5.6: Total entropy production (TEP) in the reference heat exchanger, Case 2.

TEP	**Value**	**Unit**
Total	12.5340	J/Ks
Heat	5.4540	J/Ks
Reaction	6.9953	J/Ks
Pressure drop	0.0847	J/Ks

which in the end, reduces the total entropy production. In this 80 bar case, the heat capacity is considerably lower than in the 20 bar case

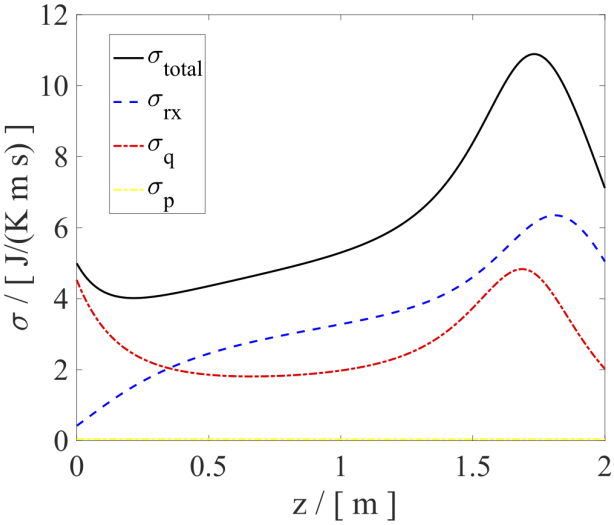

Figure 5.24: Local entropy production (LEP) of the reference heat exchanger as a function position. The yellow dot-dashed line represents the LEP associated with frictional flow, the red dot-dashed line represents the heat transfer contribution to the LEP and the blue dashed line represents the contribution form the hydrogen spin-isomer conversion reaction to the LEP. The black solid line is the sum of the three contributions, Case 2.

(see Figure 5.2 and Figure 5.5). This allows the system to have a smaller heat transfer coefficient without increasing ΔT.

We also note that the entropy production associated with the spin-isomer reaction does not undergo any big changes when the pressure is increased.

The last property of the 80 bar reference case that we are going to discuss is the density, which is considerably higher in the 80 bar case (see figure 5.4). In our system, we fix the molar flow rate, meaning that

there is a constant amount of hydrogen flowing through the system as a function of time. Thus, the velocity decreases when the density increases. This is why the entropy production related to the pressure drop almost disappears in this case.

5.3.2 The Optimal Path

An optimization was performed on the 80 bar reference case presented in section 4.2. In the optimization, all boundary conditions were fixed according to Table 4.4 except the outlet pressure, which was kept free to be optimized by the optimization program. This resulted in a new outlet pressure which is slightly increased from $79.884 \cdot 10^5$Pa to $79.885 \cdot 10^5$Pa.

The optimized temperature profiles of Case 2 is given in Figure 5.25. We notice rather linear temperature profiles compared to the 20 bar case, where we had the "plateau" in the middle of the heat exchanger. This plateau was caused by a peak in the heat capacity. In the 80 bare case, there is no peak in the heat capacity and we do not have a plateau in our temperature profiles.

Table 5.7: Total entropy production (TEP) in the optimized heat exchanger, Case 2.

TEP	**Value**	**Unit**
Total	12.2641	J/Ks
Heat	5.3922	J/Ks
Reaction	6.7875	J/Ks
Pressure drop	0.0843	J/Ks

Figure 5.26 shows the optimized local entropy production for Case 2, and Table 5.7 give the total entropy production of the system. As

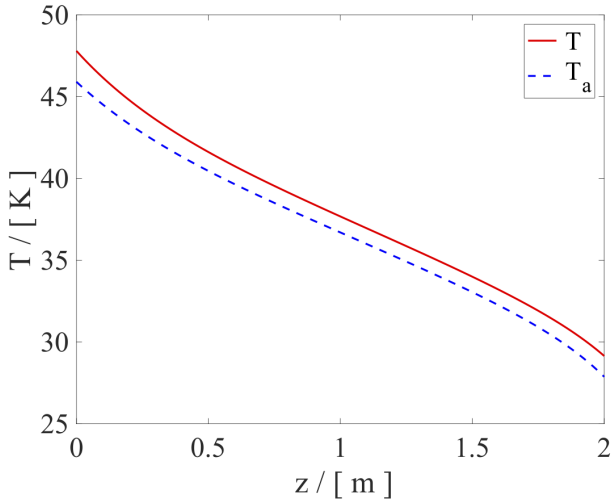

Figure 5.25: Optimized temperature profiles as a function of position, Case 2. The red solid line is the temperature (T) inside the heat exchanger and the dashed blue line is the temperature of the utility (T_a).

already discussed for the reference case, the heat transfer term is lower than for Case 1, due to a lower heat transfer coefficient and a lower and more constant heat capacity.

One quite interesting property with this case is that the reference case is quite close to the optimized case. The optimization only reduces the total entropy production by 2.15%. As described in section 4, the reference system is a system where the cold side (the utility) is hydrogen gas. In the optimization, we treat the utility as a cooling medium which can take all temperatures. As the total entropy production of the reference case is close to the optimized, we can conclude that using hydrogen as a refrigerant is not a bad choice in this high pressure case.

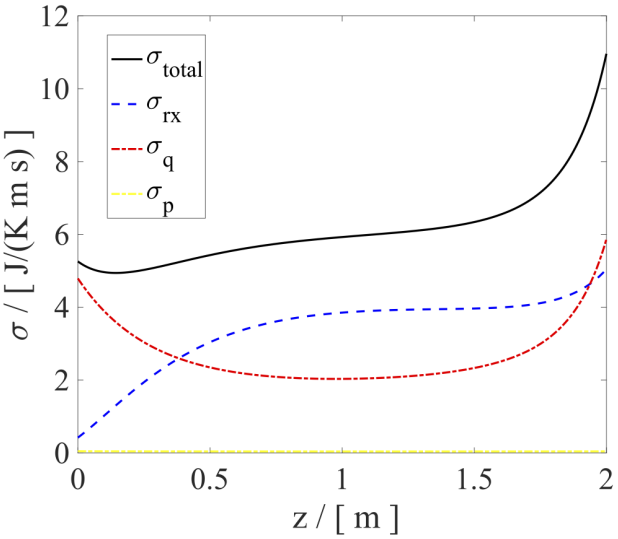

Figure 5.26: Optimized local entropy production (LEP) as a function of position, Case 2. The yellow dot-dashed line represents the LEP associated with frictional flow, the red dot-dashed line represents the heat transfer contribution to the LEP and the blue dashed line represents the contribution form the hydrogen spin-isomer conversion reaction to the LEP. The black solid line is the sum of the three contributions.

Figure 5.26 shows the same tendency as we saw in Case 2: We do not observe a reaction and a heat transfer mode. Actually, we observe something quite different. At the inlet, the heat transfer is dominating the local entropy production, and in the mid-section of the heat exchanger, the system seems to stabilize in a configuration where both the reaction and heat transfer terms are significant contributors to the entropy production.

A second general observation is that the optimal path seeks to-

wards a *more constant* local entropy production, except maybe at the boundaries. This is however just an observation, without any mathematical support, and needs to be investigated further.

The boundary effects observed in Figure 5.16 and 5.26, are caused by the fixed boundary conditions. By applying free boundary condition, these peaks can be avoided. This however will result in a higher output temperature. Increasing the output temperature will reduce the total entropy production in our heat exchanger. However, this will also "push" some of the work requirement out of this system, into another part of the hydrogen liquefaction process. This is why open boundary conditions are not considered in this study.

Comparing the total entropy production of the two cases, we note that the total entropy production of the 80 bar case is significantly lower than in the 20 bar case. This does not necessarily indicate that the 80 case is more energy efficient. When the pressure is increased, we "push" some of the work into a different section of the cooling process. In order to decide which of these cases is the most energy efficient, one has to perform an analysis on the energy demanded to increase the pressure to 80 bar.

5.3.3 The Role of a Real Gas Equation of State

As mentioned, the real gas equation of state is more expensive than the ideal gas equation of state when it comes to computational time. It is therefore interesting to use the ideal gas equation of state in the optimization and compare the results to the real gas optimization presented in the section above.

The optimized ideal gas temperature profiles of Case 2 is plotted in Figure 5.27. We notice that the difference between the two temperatures is not significantly reduced, which was the situation in Case 1. In Case 1, ΔT was reduced due to a big difference in the ideal and real gas heat capacity. As we saw in Figure 5.5, the ideal and real gas

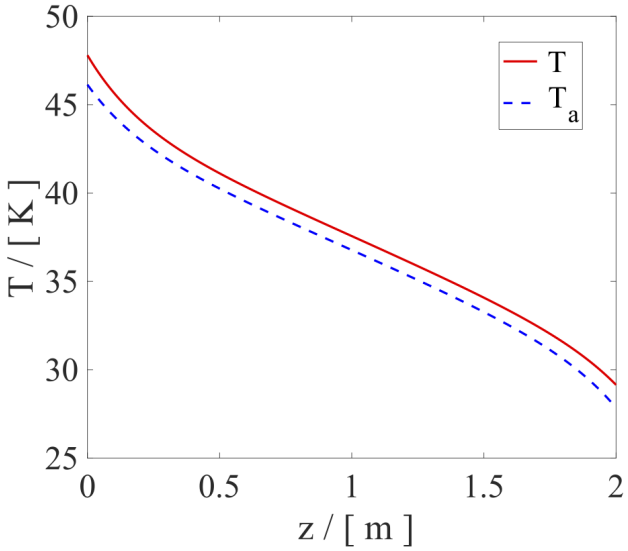

Figure 5.27: Optimized ideal gas temperature profiles as a function of position, Case 2. The red solid line is the temperature (T) inside the heat exchanger and the dashed blue line is the temperature of the utility (T_a).

heat capacity of this 80 bar case are not that different (compared to Case 1, see Figure 5.2). However, due to a lower heat capacity in the ideal gas case, the average ΔT is reduced by almost 0.2K.

This is reflected in the total entropy production given in Table 5.8. The local entropy production profiles of the real and ideal gas calculations are plotted in Figure 5.28. It looks like the local entropy production profile of the ideal gas calculations is just slightly reduced compared to the real gas calculations. The reduction is mostly due to a decline in the heat transfer term.

Figures 5.27 and 5.28 indicate that using ideal gas calculations in the 80 bar case will result in temperature profiles that are not

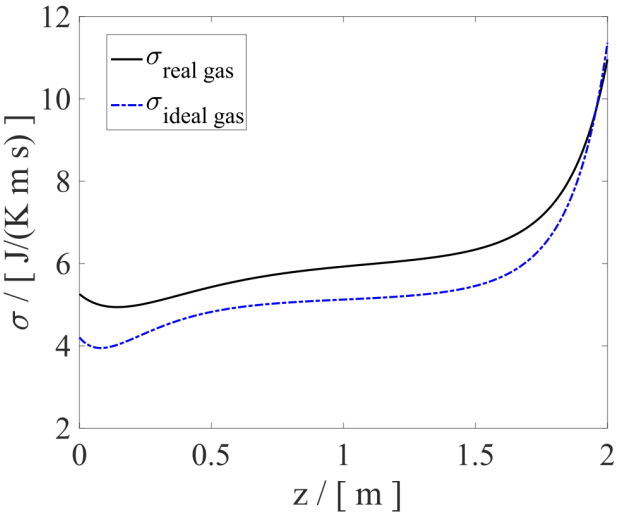

Figure 5.28: Local entropy production (LEP) as a function position, Case 2. The black solid line is the real gas LEP profile, and the dash-dotted blue line, is the ideal gas LEP profile.

Table 5.8: Total entropy production (TEP) in the optimized ideal gas heat exchanger, Case 2.

TEP	**Value**	**Unit**
Total	10.7872	J/Ks
Heat	3.8218	J/Ks
Reaction	6.8625	J/Ks
Pressure drop	0.1029	J/Ks

too far away from the real profile. However, the real gas and ideal gas profiles are not equal, and preforming an optimization using ideal gas equations will not result in the real state of minimum entropy

production.

5.3.4 Equipartition Theorems and Highway in State Space

We have seen that our system does not have the same characteristics as systems presented in literature, as we do not observe a reaction mode and a heat transfer mode. We would therefore not necessarily expect the equipartition hypothesis of Johannessen to apply. However, in Case 1, we saw that equipartition of entropy production, and also to some degree equipartition of forces, did approximate the state of minimum entropy production.

Figure 5.29 shows the temperature inside the optimized heat exchanger (black solid line), the EoEP temperature (blue dashed line) and the EoF temperature (green dot-dashed line). We observe that the EoEP and EoF temperatures do not coincide with the optimal temperature.

Figure 5.30 shows the optimized local entropy production (black solid line), the LEP profiles of the EoEP state (blue dashed line) and the LEP profiles of the EoF state (green dot-dashed line).

Table 5.9: Total Entropy Production of the reference case, optimal case, EoEP and EoF and improvement compared to the reference case, Case 2.

TEP	Value	Unit	Improvement
$\mathrm{TEP}_{Reference}$	12.5340	J/Ks	-
$\mathrm{TEP}_{Optimal}$	12.2641	J/Ks	2.15 %
TEP_{EoEP}	12.9501	J/Ks	-3.32 %
TEP_{EoF}	13.6036	J/Ks	-8.53 %

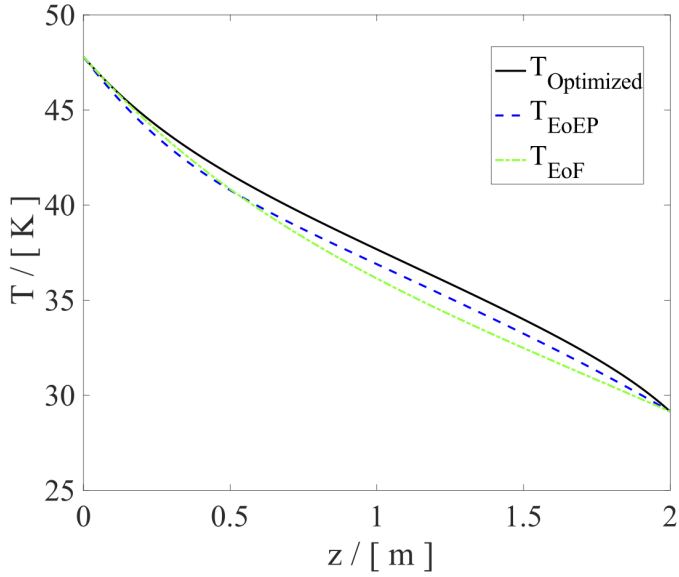

Figure 5.29: Temperature profile of the optimized case (black solid line), the EoEP temperature profile(blue dashed line) and the EoF temperature profile (green dot-dashed line) as a function of position, Case 2.

Table 5.9 gives the total entropy production together with the improvement compared to the reference case. The first thing we notice is that the total entropy production of the reference case is smaller than the total entropy production of both the EoEP and the EoF cases. As mentioned, in the reference case hydrogen gas is used as refrigerant. The fact that the reference case is so close to the optimal case is a nice and convenient coincidence which indicates that hydrogen would be a good choice as refrigerant for this particular pressure rations between the hot and cold layers.

The difference between total entropy production of the EoEP state

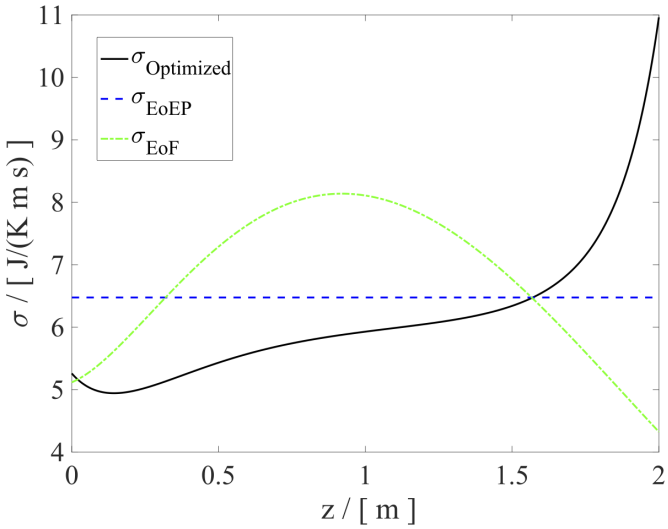

Figure 5.30: Local entropy production (LEP) of the optimized case (black solid line), the EoEP LEP profile (blue dashed line) and the EoF LEP profile (green dot-dashed line) as a function of position, Case 2.

and the optimal state is 5.59%, and for EoF, the difference is 10.92%. We observe that in this 80 bar case, EoEP and EoF do not approximate the optimal solutions good as in Case 1. This may indicate that the system does not have enough freedom for Johannessens hypothesis (cited in section 2.3.2) to apply. As we saw in Case 1, both the spin-isomer reaction and the heat transfer will be important properties through the heat exchanger, which results in a system with too few control variables. The lack of enough freedom in the system could also be caused by be the boundary conditions or the nonlinear flux-force relations (see Table 2.1).

Figure 6.1 shows six out of 30 optimizations preformed on reference Case 2 with different temperature boundary conditions. In the optimizations, the inlet pressure is fixed to 80 bar, but the outlet pressure is free.

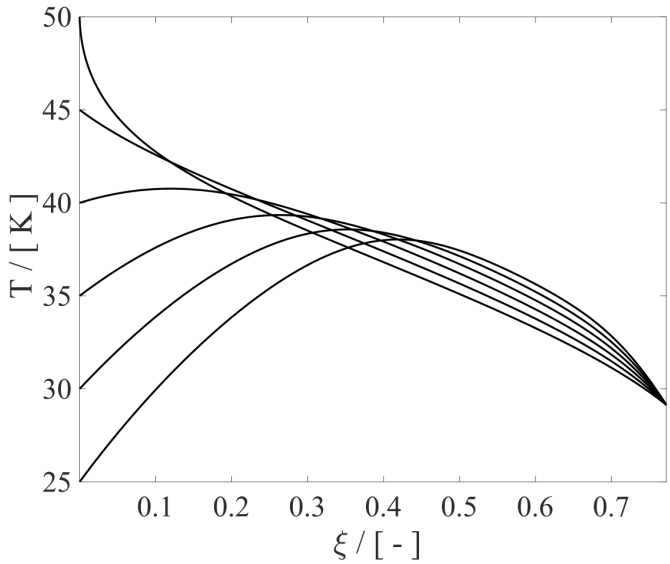

Figure 5.31: Optimized temperature profiles for different inlet temperatures as a function of the degree of reaction. The inlet temperatures plotted in the figure is: $T^0 = 50$K, $T^0 = 45$K, $T^0 = 40$K, $T^0 = 35$K, $T^0 = 30$K, $T^0 = 25$K, Case 2.

As discussed in section 5.2.4, the highway is characterized by the reaction mode. As there is no reaction mode, we would not expect the system to have a highway, which is what we observe in Figure 6.1. The system seems to organize in parallel lines, but this is however not the same as a highway.

We have now discussed two different hydrogen plate fin heat exchangers. The first heat exchanger had an inlet pressure of 19.6 bar. This case was called Case 1 or the 20 bar case. The second heat exchanger had an inlet pressure of 80.0 bar. This case was called Case 2 or the 80 bar case.

We have seen that the hydrogen liquefier have different propperites than reactors/heat exchangers studied before, where the main difference is that we do not observe a reaction and heat transfer mode in the hydrogen liquefer.

Chapter 6

Conclusion

In this thesis we have studied low temperature cooling of hydrogen gas from about 47K to 29K, which is a part of the hydrogen liquefaction process. Liquid hydrogen can be used as fuel and may in the future be able to replace fossil fuels in for example utility vehicles. In order to make hydrogen a competitive energy carrier we need to reduce the lost work in the production of liquid hydrogen.

We have modeled a plate fin heat exchanger filled with catalyst pellets in some of the layers. The plate fin heat exchanger is composed of alternating layers of hot and cold streams. The heat exchanger is chosen as its finned geometry results in a large heat exchange area to volume ratio which enables heat transfer at small temperature differences. Hydrogen is flowing in the layers filled with catalyst pellets. This is the hot stream. The cold stream is a cooling medium. This could for example be compressed hydrogen gas or mixtures such as a combination of helium and neon.

By using optimal control theory, we have studied the state of minimum entropy production in two hydrogen plate fin heat exchangers

operating at different conditions. The first heat exchanger had an inlet pressure of 19.6 bar. We called this case the 20 bar case. The second heat exchanger had an inlet pressure of 80 bar. This case was called the 80 bar case. We have found the most energy efficient designs of the hydrogen heat exchangers and compared the results to two reference cases (one for each case). In the reference cases, hydrogen gas was used as cooling medium. In the optimizations, there was no restrictions on what temperatures the cooling medium could take.

In the 20 bar case, the total entropy production was reduced from 20.2799J/Ks to 17.2582J/Ks which is an improvement of 14.90%. In the 80 bar case the total entropy production was reduced from 12.5340J/Ks to 12.2641J/Ks which is a reduction of 2.15%. This finding indicates that hydrogen, the baseline reference, could make a good candidate for refrigerant in hydrogen liquefaction at 80 bar.

We also note that the total entropy production of the 80 bar case is lower than the total entropy production of the 20 bar case. This does not necessarily mean that the 80 bar case is more efficient, as increasing the pressure may cause additional work upstream of the heat exchanger.

To give an indication of the value gained by using the computationally expensive real gas equation of state, the results were compared to optimizations with the ideal gas approximation. In both the cases, the ideal gas calculations did not find the same path as the real gas calculation. This proves that using real gas equation of state is necessary in order to find the real state of minimum entropy production.

The optimized results were also compared to similar studies given in literature. Earlier studies on entropy production minimization have reported that optimal reactors/heat exchangers can be characterized by two modes. These are the reaction and heat transfer modes. When

the system is in the reaction mode, the (chemical) reaction is dominating the system. When the system is in the heat transfer mode, the heat transfer is dominating the system.

These modes are not present in the hydrogen liquefier. This is due to the slow and temperature dependent nature of the hydrogen spin-isomer reaction. As a result of this, both the reaction and heat transfer terms of the entropy production are almost equal contributors to the entropy production through the heat exchanger. Thus, the systems do not have enough freedom for the equipartition theorems to apply, and we do not have sections with constant entropy production and constant thermodynamic forces. An other side effect of there being no heat transfer modes in the optimized heat exchangers is that there are no highways in state space. However, we have seen that the equipartition theorems can (to some degree) approximate the optimal solution as predicted by Johannessen et al. [29]. In the 20 bar case, the total entropy production obtained by using the theorem of equipartition of entropy production (EoEP) only deviated with 2.39% from the optimal, and for the theorem of equipartition of forces (EoF) the deviation was 5.24%.

In our hydrogen liquefaction heat exchanger, we have observed some rather different results than earlier studies on entropy production minimization have reported. In the future, it would be interesting to study system with similar slow and temperature dependent reactions, in order to understand these systems better.

We hope that our contribution to the design of the cryogenic hydrogen heat exchanger will help reduce the lost work in the production of liquid hydrogen.

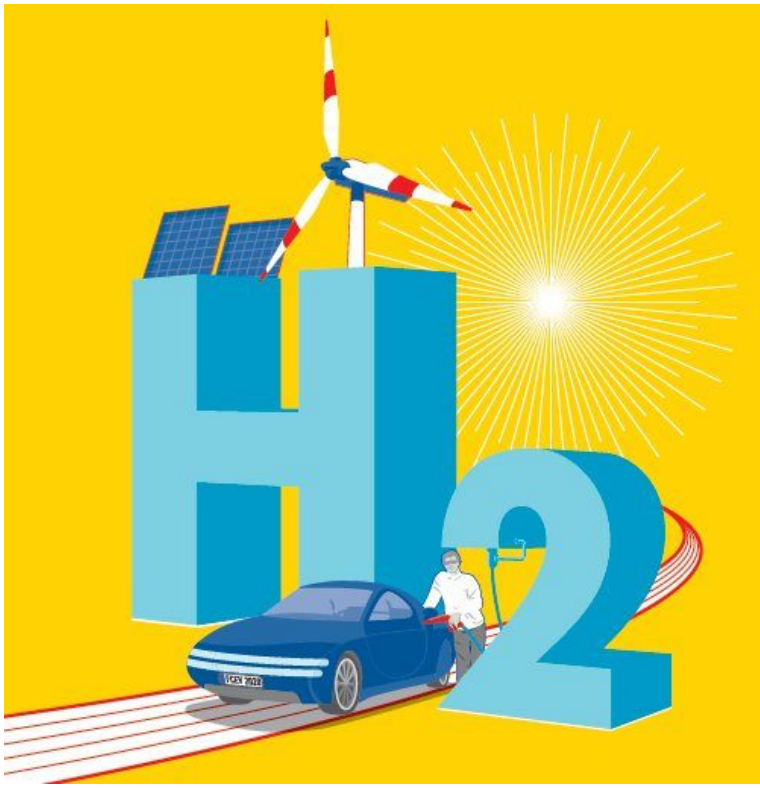

Figure 6.1: [48]

Bibliography

[1] European commision, Paris Agreement. Available at: https://ec.europa.eu/clima/policies/international/negotiations/paris_en, Visited: 26.04.2018

[2] U.S Energy Information Administration: International Energy Outlook 2017, Available at: https://www.eia.gov/outlooks/ieo/, Visited: 24.01.2018

[3] BP Statistical Review of World Energy June 2017, Available at: https://www.bp.com/en/global/corporate/energy-economics/statistical-review-of-world-energy/primary-energy.html, Visited: 26.04.2018

[4] International Energy Agency (IEA). Energy technology perspectives 2015. 2015. Paris

[5] SINTEF. HYPER. Available at: https://www.sintef.no/prosjekter/hyper/, Visited: 18.05.2018

[6] Züttel, A; Borgschulte, A; Schlapbach, L: *Hydrogen as a Future Energy Carrier*, Wiley - VCH, 2008

[7] Hemmer, P. C: *Kvantemekanikk*, Fifth edition, Tapir akademisk forlag, 2005

[8] Leachman, J. W.; Jacobes, R. T.; Penoncello, S. G.; Lemmon, E. W.: Fundamental Equations of State for Parahydrogen, Normal Hydrogen, and Orthohydrogen, *J. Phys. Chem. Ref. Data*, **2009** 38, 721 - 748

[9] Farkas, A.: *Orthohydrogen, Parahydrogen and Heavy Hydrogen*, Cambridge University Press, Cambridge, 1935

[10] Aasadina, M; Mehrpooya, M.: Large-scale liquid Hydrogen production methods and approaches: A review, *Applied Energy*, **2018** 212, 57 - 83

[11] Berstad, D. O.; Stang, J. H.; Nekså, P.: Comparison criteria for large-scale hydrogen liquefaction processes, *International Journal of Hydrogen Energy*, **2009** 34(3), 1560 - 1568

[12] Wilhelmsen, Ø.; Berstad, D.; Aasen, A.; Nekså, P.; Skaugen, G.: Reducing the exergy destruction in the cyrogenic heat exchangers of hydrogen liquefaction processes, *International Journal of Hydrogen Energy*, **2018** 43(10), 5033 - 5047

[13] Johannessen, E.: *The state of minimum entropy production in an optimally controlled system.* Doctor thesis, Norwegian University of Science and Technology, October 2004.

[14] Bejan, A: *Entropy Generation Minimization: The Method of Thermodynamic Optimization of Finite-Size Systems and Finite-Time Processes*, First edition. CRC Press, 1996

[15] Berstad, D. O.; Stang, J. H.; Nekså, P.: Large-scale hydrogen liquefier utilising mixed-refrigerant pre-cooling, *International Journal of Hydrogen Energy*, **2010** 35(10), 4512 - 4523

[16] Røsjorde, A.; Kjelstrup, S.; Johannessen, E.: Minimizing the entropy production in a chemical process for dehydrogenation of propane, *Energy*, **2007** 32(4), 335 - 343

[17] de Koeijer, G.; Johannessen, E.; Kjelstrup, S.: The second law optimal path ofa four-bed SO2 converter with five heat exchangers, *Energy*, **2004** 29, 525 - 546

[18] de Koeijer, G.; Røsjorde, A.; Kjelstrup, S.: Distribution of heat exchange in optimum diabatic distillation columns, *Energy*, **2004** 29, 2425 - 2440

[19] Magnanelli, E.; Johannessen, E.; Kjelstrup, S.: Entropy Production Minimization as Design Principle for Membrane Systems: Comparing Equipartition Results to Numerical Optima, *Ind. Eng. Chem. Res.*, **2017** 56, 4856 - 4866

[20] Sauar, E.; Kjelstrup, S. R.; Lien, K. M.: Equipartition of Forces: A New Principle for Process Design and Optimization, *Ind. Eng. Chem. Res.*, **1996** 35(11), 4147 - 4153

[21] Sauar, E.; Kjelstrup, S. R.; Lien, K. M.: Equipartition of Forces: Extension to chemical reactors, *Computers & Chemical Engineering*, **1997** 20, 29 - 34

[22] Nummedal, L.; Kjelstrup, S.:Equipartition of forces as a lower bound on the entropy production in heat exchange, *International Journal of Heat and Mass Transfer*, **2001** 15, 2827 - 2833

[23] Andresen, B.; Gordon, J. M.: Constant thermodynamic speed for minimizing entropy production in thermodynamic processes and simulated annealing, *Phys. Rev. E*, **1994** 50, 4346

[24] Tondeur, D.; Kvaalen, E.: Equipartition of Entropy Production. An Optimality Criterion for Transfer and Separation Processes, *Ind. Eng. Chem. Res.*, **1987** 26, 50 - 56

[25] Spirkl, W.; Ries, H.: Optimal Finite-Time Endoreversible Processes, *Phys. Rev. E*, **1995** 52, 3485 - 3489

[26] Wilhelmsen, Ø.; Johannessen, E.; Kjelstrup, S: Energy efficient reactor design simplified by second law analysis, *International Journal of Hydrogen Energy*, **2010** 35, 13219 - 13231

[27] Johannessen, E.; Nummedal, L.; Kjelstrup, S.: Minimizing the entropy production in heat exchange, *International Journal of Heat and Mass Transfer*, **2002** 45(13), 2649 - 2654

[28] Johannessen, E.; Kjelstrup, S.: A highway in state space for reactors with minimum entropy production, *Chemical Engineering Science*, **2005** 60(12), 3347 - 3361

[29] Johannessen, E.; Kjelstrup, S.: Minimum entropy production rate in plug flow reactors: An optimal control problem solved for SO2 oxidation, *Energy*, **2004** 29(12-15), 2403 - 2423

[30] Nummedal, L.; Rørsjorde, A.; Johannessen, E.; Kjelstrup, S.: Second law optimization of a tubular steam reformer, *Chemical Engineering and Processing: Process Intensification*, **2005** 44(4), 429 - 440

[31] Fogler, S. H.: *Elements of Chemical Reaction Engineering*, Fourth edition. Person International Edition, 2005

[32] Callen, H. B.: *Thermodynamics and an introduction to thermostatistics*, Second edition, Wiley, 1985

[33] Roy, B. N: *Fundamentals of Classical and Statistical Thermodynamics*, First edition, Wiley, 2002

[34] National Institute of Standards and Technology (NISR) REFPROP. Available at:
`https://www.nist.gov/srd/refprop`, Visited: 29.04.2018

[35] Selander, W. N: *Explicit formulas for the computation of friction factors in turbulent pipe flow*, Atomic Energy of Canada Ltd, **1978** Report AECL-6354, Chalk River Nuclear Laboratories, Chalk River, Ontario

[36] Voldsund, M.; Jordal, K.; Anantharaman, R.: Hydrogen production with CO2 capture *International Journal of Hydrogen Energy* **2016** 41, 4969 - 4992

[37] Hemmer, P. C: *Termisk Fysikk*, Second edition, Tapir akademisk forlag, 2009

[38] Hutchinson, H. L.; Brown, L. F.; Barrick, P. L.: A comparison of rate expressions for the low-temperatur para-orthohydrogen shift, *Advances in Cryogenic Engineering*, **1971** 16, 96 - 103

[39] Kjelstrup, S; Bedeaux, D; Johannessen, E; Gross, J: *Non-Equalibrium Thermodynamics for Engineers*, Second edition. World Scientific, 2017

[40] Lemmon, E. W.; Jacobes, R. T.: A New Functional Dorm and New Fitting Techniques for Equations of State with Applications to Pentafluoroethane (HFC-125), *J. Phys. Chem. Ref. Data*, **2005** 34, 69 - 108

[41] Pontryagin, L. S; Boltyanskii, V. G; Gamkrelidze, R. V; Mishchenko, F. F: *The Mathematical Theory of Optimal Processes*, First edition, Tapir John Wiley and Sons, 1963

[42] Sadaghiania, M. S.; Mehrpooya, M.: Introducing and energy analysis of a novel cryogenic hydrogen liquefaction process configuration, *International Journal of Hydrogen Energy*, **2017** 42, 6033 - 6050

[43] Span, R.: *Multiparameter Equation of State*. Springer, 2000

[44] Shultz, M: *Control Theory in Physics and other Fields of Science*, First edition, Springer, 2006

[45] Younglove, B. A.; *Thermophysical Properties of Fluids. I. Argon, Ethylene, Parahydrogen, Nitrogen, Nitrogen Trifluoride, and Oxygen*, National Standars Reference Data System, 1982

[46] Salamon, P.; Nitzan, A.; Andresen, B.; Stephen, B. R.: Minimum entropy production and the optimization of heat engines, *Phys. Rev. A*, **1980** 21, 2115 - 2129

[47] Peters, P. E.; Schiffino, R. S.; Harriott, P.: Heat transfer in packed-tube reactors, *Industrial & Engineering Chemistry Fundamentals*, **1988** 27, 226 - 233

[48] Shell, Hydrogen's role in the future of transport: Available at: `https://www.shell.com/energy-and-innovation/the-energy-future/future-transport/hydrogen.html`, Visited: 27.05.2018

Appendix A

Calculation Details

A.1 Equation of state

In the multiparameter equation of state formulation, the pressure(P) entropy (s), enthalpy (h) and heat capacity (c_p) are given through the Helmholtz energy (a). To simplify the calculations, all the themodynamic variables are given in reduced (dimentionless) form.

As discussed in section 2.4, the reduced Helmholtz energy, α, is given by

$$\alpha(\delta, \tau) = \frac{a(P,T)}{RT} = \alpha^0(\delta, \tau) + \alpha^r(\delta, \tau). \tag{A.1}$$

Here, $\delta = \rho/\rho_0$ and $\tau = T_c/T$, are reduced density and temperature. α^0 is the ideal contribution to the Helmholtz energy given in equation A.2 and repeted here,

$$\alpha^0(\delta, \tau) = \ln \delta + 1.5 \ln \tau + a_1 + a_2\tau + \sum_{k=3}^{N} a_k \ln[1 - e^{b_k \tau}], \tag{A.2}$$

and α^r is the residual contribution given by equation A.3, and also repeted here,

$$\alpha^r(\delta,\tau) = \sum_{i=1}^{l} N_i \tau^{t_i} \delta^{d_i} + \sum_{i=l+1}^{m} N_i \tau^{t_i} \delta^{d_i} e^{-\delta^{p_i}} + \sum_{i=m+1}^{n} N_i \tau^{t_i} \delta^{d_i} e^{\phi_i(\delta - D_i)^2} e^{\beta_i(\tau-\gamma_i)^2}. \tag{A.3}$$

The Helmholtz energy is the fundament for all thermodynamic calculations in the hydrogen system. We will here list the necesary equations for pressure, entropy, enthalpy and heat capacity. Similar equations and more details can be fond in the article of Lemmon et al. [40] or in the textbook by Span on Multiparameter Eqautions of State [43].

The pressure is given by

$$P = \rho^2 \left(\frac{\partial a}{\partial \rho}\right)_T = \frac{\rho^2}{\rho_c} RT \frac{\partial \alpha}{\partial \delta} = \delta^2 \rho_c RT \frac{\partial \alpha}{\partial \delta} \tag{A.4}$$

The entropy is given by

$$\frac{s}{R} = \tau \left[\left(\frac{\partial \alpha^0}{\partial \tau}\right)_\delta + \left(\frac{\partial \alpha^r}{\partial \tau}\right)_\delta \right] - \alpha^0 - \alpha^r. \tag{A.5}$$

The enthalpy is given by

$$\frac{h}{RT} = \tau \left[\left(\frac{\partial \alpha^0}{\partial \tau}\right)_\delta + \left(\frac{\partial \alpha^r}{\partial \tau}\right)_\delta \right] + \delta \left(\frac{\partial \alpha^r}{\partial \delta}\right)_\tau + 1. \tag{A.6}$$

The heat capacity is given by

$$\frac{c_p}{R} = \frac{c_v}{R} + \frac{\left[1 + \delta\left(\frac{\partial \alpha^r}{\partial \delta}\right)_\tau - \delta\tau\left(\frac{\partial^2 \alpha^r}{\partial \delta \partial \tau}\right)\right]^2}{\left[1 + 2\delta\left(\frac{\partial \alpha^r}{\partial \delta}\right)_\tau - \delta^2\left(\frac{\partial^2 \alpha^r}{\partial \delta^2}\right)_\tau\right]}, \tag{A.7}$$

where c_v is given by

$$\frac{c_v}{R} = -\tau^2\left[\delta\left(\frac{\partial^2 \alpha^0}{\partial \tau^2}\right)_\delta + \left(\frac{\partial^2 \alpha^r}{\partial \tau^2}\right)_\delta\right]. \tag{A.8}$$

A.2 Derivatives of Helmholtz Energy

As the observant reader probably allrady noticed, all themodynamic properties are givs as derivatives of the reduced Helmholtz energy, and it will therfore be necessary to do the following derivatives. All parameters are given in the article by Leachman et al. [8].

The derivatives of $\alpha^{\mathbf{r}}$:

$$\left(\frac{\partial \alpha^r}{\partial \delta}\right)_\tau = \sum_{i=1}^{l} N_i \tau^{t_i} d_i \delta^{d_i - 1} + \sum_{i=l+1}^{m} N_i \tau^{t_i} \delta^{d_i - 1}[d_i - p_i \delta^{p_i}] e^{-\delta^{p_i}} + \sum_{i=m+1}^{n} N_i \tau^{t_i} \delta^{d_i - 1}[d_i + 2\phi_i \delta(\delta - D_i)] e^{\phi_i (\delta - D_i)^2} e^{\beta_i (\tau - \gamma_i)^2}.$$

$$\left(\frac{\partial \alpha^r}{\partial \tau}\right)_\delta = \sum_{i=1}^{l} N_i \tau^{t_i - 1} \delta^{d_i} t_i + \sum_{i=l+1}^{m} N_i \tau^{t_i - 1} \delta^{d_i} e^{-\delta^{p_i}} t_i + \sum_{i=m+1}^{n} N_i \tau^{t_i - 1} \delta^{d_i}[t_i + 2\beta_i \tau(\tau - \gamma_i)] e^{\phi_i (\delta - D_i)^2} e^{\beta_i (\tau - \gamma_i)^2}.$$

$$\left(\frac{\partial^2\alpha^r}{\partial\delta^2}\right)_\tau = \sum_{i=1}^{l} N_i\tau^{t_i}\delta^{d_i-2}d_i(d_i-1)$$
$$+ \sum_{i=l+1}^{m} N_i\tau^{t_i}\delta^{d_i-2}\Big[d_i(d_i+1) - p_i\delta^{p_i}(2d_i-1+p_i(1-\delta^{p_i}))\Big]e^{-\delta^{p_i}}$$
$$+ \sum_{i=m+1}^{n} N_i\tau^{t_i}\delta^{d_i-2}\Big[d_i(d_i-1)$$
$$+ 2\phi_i\delta\big[2d_i(\delta-D_i) + 2\phi_i\delta(\delta-D_i)^2+\delta\big]\Big]e^{\phi_i(\delta-D_i)^2}e^{\beta_i(\tau-\gamma_i)^2}.$$

$$\left(\frac{\partial^2\alpha^r}{\partial\tau^2}\right)_\delta = \sum_{i=1}^{l} N_i\tau^{t_i-2}\delta^{d_i}t_i(t_i-1)$$
$$+ \sum_{i=l+1}^{m} N_i\tau^{t_i-2}\delta^{d_i}t_i(t_i+1)e^{-\delta^{p_i}}$$
$$+ \sum_{i=m+1}^{n} N_i\tau^{t_i-2}\delta^{d_i}\Big[t_i(t_i-1)$$
$$+ 2\beta_i\tau\big[2t_i(\tau-\gamma_i) + 2\beta_i\tau(\tau-\gamma_i)^2+\tau\big]\Big]e^{\phi_i(\delta-D_i)^2}e^{\beta_i(\tau-\gamma_i)^2}.$$

$$\left(\frac{\partial^2\alpha^r}{\partial\delta\partial\tau}\right) = \sum_{i=1}^{l} N_i\tau^{t_i-1}\delta^{d_i-1}t_i d_i + \sum_{i=l+1}^{m} N_i\tau^{t_i-1}\delta^{d_i-1}t_i[d_i - p_i\delta^{p_i}]e^{-\delta^{p_i}} + \sum_{i=m+1}^{n} N_i\tau^{t_i-1}\delta^{d_i-1}[t_i + 2\beta_i\tau(\tau-\gamma_i)] \times [d_i + 2\phi_i\delta(\delta - D_i)]e^{\phi_i(\delta-D_i)^2}e^{\beta_i(\tau-\gamma_i)^2}.$$

Derivatives of $\alpha^{\mathbf{0}}$:

$$\left(\frac{\partial\alpha^0}{\partial\tau}\right)_\delta = \frac{1.5}{\tau} + a_2 - \sum_{k=3}^{N} a_k\frac{b_k e^{b_k\tau}}{1-e^{b_k\tau}}$$

$$\left(\frac{\partial^2\alpha^0}{\partial\tau^2}\right)_\delta = -\frac{1.5}{\tau^2} - \sum_{k=3}^{N} a_k\frac{b_k^2 e^{b_k\tau}}{\left(1-e^{b_k\tau}\right)^2}$$

A.3 The Real Gas Density of Hydrogen Gas

The Hemholtz energy depends on the density ρ. In this system, the density is not given explicitly, but implicitely through equation (A.4). One method frequantly used to solve such equations is newtons method, which is an iterative method used to find the roots of a function.

We start by defining ourself a function $f(\delta)$. In our case, $f(\delta)$ is a reorganized version of equation (A.4) given by

$$f(\delta) = \frac{\partial \alpha}{\partial \delta} - P\frac{1}{\delta^2 \rho_c RT} = \frac{\partial \alpha^0}{\partial \delta} + \frac{\partial \alpha^r}{\partial \delta} - P\frac{1}{\delta^2 \rho_c RT} = 0. \tag{A.9}$$

The aim of newtons method is to find a δ which results in a $f(\delta)$ sufficciently close to zero. Newtons method is composed of four steps

1. Guess a solution to the problem $f(\delta) = 0$. We call this solution δ_1. In our case, the initial guess is obtained by using the ideal gas expression for the density.

2. Find a linearization of $f(\delta)$ at δ_1. The linearization is given by $L(\delta) = f(\delta_1) + f'(\delta_1)(\delta - \delta_1)$.

3. Solve $L(\delta) = 0$, and call the solution δ_2. Solving $L(\delta) = 0$ is equivalent to sloving $\delta_2 = \delta_1 - \frac{f(\delta_1)}{f'(\delta_1)}$.

4. Repeat 2 and 3 until $f(\delta)$ is sufficiantly close to zero. In our case, the tolerence is 10^{-12}.

In order to do this we need the derivative of equation A.9.

$$f'(\delta) = \frac{\partial^2 \alpha}{\partial \delta^2} + P\frac{2}{\delta^3 \rho_c RT} = \frac{\partial^2 \alpha^0}{\partial \delta^2} + \frac{\partial^2 \alpha^r}{\partial \delta^2} + P\frac{2}{\delta^3 \rho_c RT} \tag{A.10}$$

A.4 Reaction rate

The reaction rate of the ortho-para conversion (1.1) is an imprtant property and it appears in the balance equations for energy and mass, as well as in the entropy production equation. Hutchinson et al. [38] developed in 1971 an expression for the reaction rate for the ortho-para conversion

$$r_{o\to p} = K \ln\left[\left(\frac{x_{H_{2,p}}}{x^{eq}_{H_{2,p}}}\right)^n \left(\frac{1-x^{eq}_{H_{2,p}}}{1-x_{H_{2,p}}}\right)\right]. \tag{A.11}$$

Here K and n are parameters, $x_{H_{2,p}}$ is the mole fraction and $x^{eq}_{H_{2,p}}$ is the equilibrium mole fraction which is given in [12] as

$$\begin{aligned} x^{eq}_{H_{2,p}} = 0.1\left[\exp\left(\frac{-5.313}{\tau}\right) + 0.1\right]^{-1} - 2.52\cdot 10^{-4}\tau^3 \\ + 3.71\cdot 10^{-3}\tau^2 - 2.04\cdot 10^{-3}\tau - 0.00227. \end{aligned} \tag{A.12}$$

Here $\tau = T/T_c$ where T is the temperature and T_c it the critical temperature. The parameter K is given by

$$K = b + c\cdot\tau + d\cdot\rho \tag{A.13}$$

where b, c and d are parameters and $\rho = P/P_c$. P_c is the critical pressure and all the other parameters are given by Wilhelmsen et al. [**?**], and repeted here in Table A.1.

Table A.1: Reaction Rate parameters and critical values.

parameter	value	unit
T_c	32.937	K
P_c	1.28377	MPa
n	1.0924	-
b	0.0597	mol/(m^3s)
c	-0.2539	mol/(m^3s)
d	-0.0116	mol/(m^3s)